Altered laminin signaling destinates melanocyte reprogramming in vitiligo

Fei Yang [1,2], Lingli Yang [1*], Sylvia Lai [1], Masafumi Yokota [1,2], Yasutaka Kuroda [1,2], Takuo Yuki [2], Yoshito Takahashi [2], Tetsuya Sayo [2], Takeshi Namiki [3], Hiroyuki Goto [4], Sho Hiroyasu [4], Shigetoshi Sano [5], Shintaro Inoue [6], Yoichi Mizukami [7], Daisuke Tsuruta [4] and Ichiro Katayama [1]

[1] Department of Pigmentation Research and Therapeutics, Graduate School of Medicine, Osaka Metropolitan University, Osaka, Japan
[2] Cosmetic Product Research, Research and Development, Kao Corporation, Odawara, Japan
[3] Department of Dermatology, Graduate School and Faculty of Medicine, Institute of Science Tokyo, Tokyo, Japan
[4] Department of Dermatology, Graduate School of Medicine, Osaka Metropolitan University, Osaka, Japan
[5] Department of Dermatology, Kochi Medical School, Kochi University, Kochi, Japan
[6] Department of Cosmetic Health Science, Gifu Pharmaceutical University, Gifu, Japan
[7] Institute of Gene Research, Yamaguchi University Science Research Center, Yamaguchi, Japan

[*] Correspondence to: L Yang, Department of Pigmentation Research and Therapeutics, Graduate School of Medicine, Osaka Metropolitan University, Osaka 5450051, Japan. E-mail: yang.lingli@omu.ac.jp.

Manuscript word:8148 Figure counts: 6 Supplementary figure counts: 22 **Supplementary table counts:** 8
Funding sources: This research was supported by JSPS KAKENHI Grant Numbers 22K08409 and 18K08267.
Conflicts of interest: The authors declare no conflict of interest.
Ethics statement: The specimen collection and overall study design were approved by the Medical Ethics Committee of Osaka Metropolitan University (No. 4152).

Abstract

Vitiligo is an autoimmune skin disorder characterized by progressive melanocyte loss, yet its underlying mechanisms remain unclear. Likewise, the specific molecules and mechanisms mediating melanocyte adhesion to the basement membrane (BM) are poorly understood despite their essential role in skin homeostasis. Here, we identify dystroglycan-laminin-211 as the primary adhesion mechanism anchoring melanocytes to the BM in normal skin. In vitiligo, this adhesion shifts to integrin α3β1-laminin-332 binding. This transition activates the Hippo and MAPK pathways via Rho-F-actin signaling, inducing c-JUN-mediated dedifferentiation and neural crest-like reprogramming. Dedifferentiated melanocytes lose their epidermal identity, acquire multi-lineage potential, and resist repigmentation. Pharmacological inhibition of this dedifferentiation process restores pigmentation in leukoderma models and skin explants from the patient with vitiligo. Notably, JAK inhibitors directly promote melanocyte differentiation, independent of any immunomodulation. These findings identify melanocyte reprogramming as a central pathogenic mechanism in vitiligo and provide novel therapeutic strategies targeting adhesion and fate for disease intervention.

Introduction

Vitiligo is a chronic autoimmune disorder characterized by the progressive loss of melanocytes, resulting in depigmented skin patches that affect approximately 1% of the global population. Beyond its dermatological manifestations, vitiligo has a significant psychosocial burden on affected individuals, markedly affecting quality of life[1]. The pathogenesis of vitiligo is complex and multifactorial, involving genetic susceptibility, environmental triggers, and immune-mediated mechanisms that lead to melanocyte dysfunction and loss[2].

At present, several mechanisms have been implicated in melanocyte disappearance within vitiligo lesional skin. Direct cytotoxicity mediated by $CD8^+$ T cells and NK cells through granzyme B and perforin has been recognized as a primary mechanism of melanocyte destruction[3]. Additionally, melanocytes may detach from the basal layer and be eliminated from the skin due to changes in adhesion properties, further contributing to depigmentation[4-6]. Oxidative stress plays a crucial role, with impaired NRF2 signaling increasing melanocyte vulnerability to apoptosis[7]. Metabolic changes and defective autophagy responses also disrupt melanocyte homeostasis, resulting in cellular dysfunction and loss[8]. Furthermore, the accumulation of senescence-associated secretory phenotype (SASP) factors in aging skin has been suggested to further impair melanocyte survival[9]. Despite advances in therapeutic strategies, including immune-modulating agents and phototherapy, sustained and complete regimentation remains challenging, and no curative treatment currently exists. A more comprehensive understanding of these pathogenic mechanisms will be essential for the development of targeted and more effective therapeutic approaches.

A critical yet inadequately explored aspect of melanocyte homeostasis is their interaction with the basement membrane (BM) and its associated extracellular matrix (ECM), which are essential for maintaining melanocyte adhesion, stability, and survival[10-12]. The BM provides structural support and regulates key signaling pathways that influence melanocyte proliferation and migration. Histopathological analyses have

identified ultrastructural abnormalities in the BM of vitiligo lesions[13], suggesting that disruption of BM integrity may contribute to melanocyte detachment and loss. However, the specific molecular alterations within the BM that influence melanocyte adhesion and survival remain poorly characterized.

In our previous study[14], we demonstrated that disorganisation of the BM architecture impaired melanocyte residency in vitiligo. This unexpected observation is initiated by MMP2 activation through several inflammatory cytokines upregulated in the lesional vitiligo skin, all of those cytokines also possess inhibitory effects on melanin synthesis[15-18]. Although MMP2 activation has been known to link to excessive tissue degradation in diseases such as cancer metastasis, arthritis, and tissue fibrosis[19], there is no previous report available except for ours demonstrating the active role in vitiligo pathogenesis[14].

Among the components of the BM, laminins are key regulators of cell-matrix interactions and serve as essential constituents of the lamina lucida, the uppermost layer of the dermal-epidermal junction that interfaces directly with basal cells, including melanocytes[20]. Laminins interact with integrins and other cellular receptors to mediate adhesion, migration, and survival, with different isoforms exerting distinct functional effects. Given the diversity of laminin isoforms and their specific receptor-binding properties[21], changes in laminin composition may significantly influence melanocyte behavior and viability in vitiligo. Although previous studies have implicated various adhesion molecules in melanocyte attachment[22], the precise role of BM components, particularly laminins, in melanocyte homeostasis and vitiligo pathogenesis remains largely unexplored.

In the present study, we systematically investigate the molecular composition of the BM around melanocytes in normal and vitiligo skin. We demonstrate that melanocyte-BM interactions differ significantly between healthy and vitiliginous skin and identify distinct laminin-receptor interactions that contribute to melanocyte retention or detachment. These findings reveal previously unrecognized mechanisms underlying melanocyte loss in vitiligo and suggest potential therapeutic targets aimed at stabilizing melanocyte adhesion and promoting regimentation.

Results

Specialized laminin microenvironment defines melanocyte adhesion patterns in healthy and vitiligo

To determine the role of laminin localization in melanocyte adhesion and its implications for vitiligo, we systematically examined the localization of laminin isoforms surrounding melanocytes in healthy and perilesional vitiliginous skin (vitiligo-PL), identified the corresponding adhesion receptors, and characterized their functional roles.

Firstly, we investigated the laminin milieu surrounding melanocytes in healthy skin. Immunofluorescence analysis of healthy skin showed laminin α2, β1, and γ1 localization around melanocytes, while laminin α3, β3, and γ2 were absent (Extended Data Fig. 1, Fig. 1a). This specific laminin localization pattern appears to regulate normal melanocyte adhesion and function. In perilesional vitiligo skin, melanocytes exhibited linear laminin α3, β3, and γ2 localization without the selective absence observed in normal skin (Fig. 1a). Immuno-electron microscopy confirmed the absence of laminin α3 around normal melanocytes and its presence around vitiligo melanocytes (Fig. 1b). Although some normal melanocytes occasionally showed laminin-332 presence in immunofluorescence staining, electron microscopy revealed these cells lacked direct contact with the basement membrane, suggesting a non-adhesive interaction (Extended Data Fig. 2).

To identify the receptors involved in these interactions, we examined integrin expression in normal skin melanocytes. These cells expressed integrins α2, α5, αv, β1, β3, and, to a lesser extent, β4 (Extended Data Fig. 3). To visualize the protein-protein interactions in situ, we performed the proximity ligation assay (PLA) assay in skin tissue (Figure 1c). In keratinocyte controls, PLA assay confirmed the expected integrin-laminin interactions; however, no binding between integrins β1, β3, or β4 and laminin α2 was detected in melanocytes (Extended Data Fig. 4), suggesting alternative adhesion mechanisms between keratinocytes and melanocytes.

Considering that dystroglycan also binds laminin-211[21], we investigated its role in melanocyte adhesion. Normal melanocytes demonstrated strong dystroglycan-laminin-211 binding, whereas this interaction was markedly reduced in vitiligo melanocytes (Fig. 1d). Additionally, despite the absence of laminin α5 around

melanocytes (Extended Data Fig. 1) and previous reports of DDR1-collagen 4 in melanocyte adhesion[23], we examined these potential interactions. Both normal and vitiligo melanocytes showed minimal binding to laminin α5 and weak DDR1-collagen 4 interactions. Instead, vitiligo melanocytes primarily utilized integrin β1-laminin-332 binding (Fig. 1d). These observations reveal that in normal skin, melanocyte adhesion is mediated predominantly by dystroglycan–laminin-211 interactions, whereas in vitiligo melanocytes, the adhesion mechanism switches to laminin-332–integrin β1 interactions (Fig. 1e).

To validate dystroglycan's role in melanocyte adhesion, we employed antibody neutralization, siRNA knockdown, and enzymatic deglycosylation approaches. Treatment with anti-dystroglycan antibodies effectively inhibited melanocyte adhesion to laminin-211-coated surfaces, whereas targeting integrin α7β1, another reported laminin-211 receptor, had no significant effect. Moreover, silencing dystroglycan or its glycosylation regulator LARGE prevented adhesion to laminin-211, and enzymatic removal of dystroglycan glycosylation sites decreased melanocyte-laminin-211 binding in a dose-dependent manner (Fig. 1f).

These findings establish distinct laminin localization patterns and adhesion mechanisms between normal and vitiligo melanocytes. These differential adhesion profiles enhance our understanding of melanocyte biology and offer new insights into vitiligo pathogenesis, potentially identifying novel therapeutic targets.

Laminin-332-induced adhesion changes induce melanocyte dedifferentiation

To elucidate the functional consequences of altered cell adhesion in vitiligo melanocytes, we compared the effects of laminin-332 with those of laminin-211. Normal melanocytes treated with laminin-332 underwent dramatic morphological changes, becoming flattened and exhibiting almost undetectable levels of key melanogenic proteins such as PMEL and TRP1 (Fig. 2a).

To further characterize the subpopulation with the most pronounced alterations, we used magnetic-activated cell sorting (MACS) based on c-Kit expression, a cell surface marker of differentiated and functional melanocytes. In c-Kit–negative cells, Western blot analysis revealed a severe reduction in melanogenic proteins: DCT and tyrosinase decreased to approximately 7–8% of control (laminin-211-treated)

levels, while PMEL and TYRP1 were reduced to 10.1% and 21.1%, respectively. Even MELAN-A, which showed the least change, dropped to 52.9% of control levels. In c-Kit–positive cells, although the changes were less pronounced, a similar trend was observed (Fig. 2b). These protein level reductions were associated with a significant decrease in melanin production (Fig. 2c). This phenotype was consistently observed across five different melanocyte lines (Extended Data Fig. 5), indicating that the morphological and molecular changes to laminin-332 is a conserved response rather than a cell line-specific effect.

The dramatic phenotypic and molecular changes prompted further investigation of the underlying mechanisms. RNA sequencing and Gene Set Enrichment Analysis (GSEA) comparing laminin-332–treated and laminin-211–treated melanocytes revealed significant enrichment of pathways related to embryonic stem cell pluripotency and neural crest cell migration (Fig. 2d), suggesting a shift toward a dedifferentiated, stem cell-like state. To test this hypothesis, we evaluated the stem cell properties of laminin-332-treated melanocytes using lineage-specific differentiation assays. Under the appropriate differentiation media, these cells successfully transdifferentiated into neurons, chondrocytes, and muscle cells (Fig. 2e), thereby confirming their dedifferentiated state.

To define the extent of dedifferentiation, we compared laminin-332–treated melanocytes with cultured melanoblasts. Both cell types lacked MELAN-A expression (Extended Data Fig. 6). Although melanoblasts typically express c-Kit and DCT[24], laminin-332-induced cells exhibited heterogeneous expression, with some cells losing both markers, suggesting dedifferentiation beyond the melanoblast stage. Consistent with their neural crest origin[25], early neural crest markers such as SOX9 and NGFR were strongly expressed in both melanoblasts and laminin-332–treated melanocytes (Extended Data Fig. 6).

Detailed immunophenotyping revealed a spectrum of cellular states following laminin-332 treatment. A subset of cells retained a mature melanocyte phenotype (either DCT/c-Kit/MELAN-A triple-positive or NGFR/SOX9–negative but MELAN-A–positive) (Extended Data Fig. 7a-d, cell #1). Other cells, in transition, either maintained DCT/c-Kit positivity with loss of MELAN-A or acquired NGFR/SOX9 expression while still expressing MELAN-A (Extended Data Fig. 7a-d, cell #2). Notably, a fraction of cells appeared fully

dedifferentiated, losing all melanocytic markers (DCT/c-Kit/MELAN-A triple-negative) while expressing neural crest markers (NGFR/SOX9–positive) (Extended Data Fig. 7a-d, cell #3); some of these cells even lost neural crest marker expression (Extended Data Fig. 7c-d, arrowhead).

These results demonstrate that altered interactions with laminin-332 induce a dedifferentiated state in melanocytes, characterized by distinct molecular and phenotypic changes and a loss of melanogenic function. This dedifferentiation process offers new insights into the pathogenesis of vitiligo and may inform future therapeutic strategies aimed at restoring normal melanocyte differentiation.

Molecular mechanisms of laminin-332-induced melanocyte dedifferentiation

To investigate the molecular mechanisms underlying laminin-332-induced melanocyte dedifferentiation, we first focused on integrin-mediated signaling, as integrins are well-established receptors for laminin-332[21]. Immunostaining of cultured melanocytes demonstrated expression of integrins α3, α4, α5, α6, αv, β1, and β3 (Extended Data Fig. 8a). Since laminin-332 preferentially binds to integrin dimers containing α3, α6, and β1[21], we performed siRNA-mediated knockdown of integrins α3, α6 and β1, using integrins α1, α4, αv, and β3 siRNA as controls. Notably, silencing either integrin α3 or β1 markedly reduced the proportion of dedifferentiated cells (Extended Data Fig. 8b, where blue phalloidin-single-positive cells indicate dedifferentiation), thereby identifying integrin α3β1 complex as the primary signal transducer.

Bulk RNA-Seq analysis revealed that laminin-332-treated melanocytes exhibited a distinct transcriptional profile compared with cells treated with laminin-211, with numerous differentially expressed genes. Among the most upregulated genes were several targets of the Hippo pathway, including TGFBI, CCN1, DKK1, CCN2, and THBS1, whereas melanogenic genes (MLANA, PMEL, TYR) were downregulated (Fig. 3a). Gene Ontology enrichment analysis further confirmed significant involvement of the Hippo pathway, along with the PI3K-Akt and MAPK signaling pathways (Fig. 3b). Enrichment of cytoskeleton-related terms may also explain the observed cell flattening in Fig. 2a.

To confirm the functional significance of these pathways, we systematically knocked down key

components of the Hippo, PI3K-Akt, and MAPK pathways in laminin-332-treated melanocytes (Fig. 3c). Silencing of Hippo pathway components (YAP1, TEAD1, CCN1, CCN2) or MAPK pathway components (BRAF, ERK1, JNK1) significantly increased differentiation rates, thereby suppressing dedifferentiation (Fig. 3f). Consistent with previous reports linking MAPK signaling to dedifferentiation via AP-1 family members[26] and demonstrating that both Hippo and MAPK pathways can induce AP-1 expression[27,28], knockdown of c-JUN and c-FOS similarly inhibited dedifferentiation (Fig. 3f). In contrast, silencing of PI3K-Akt components (PIK3CA, GSK3B) or factors known to regulate differentiation, such as β-catenin (CTNNB1) and NOTCH1[29,30], did not affect laminin-332-induced dedifferentiation (Fig. 3f).

Integrin signaling is known to influence both MAPK and Hippo signaling through Rho-mediated alterations in F-actin structure [31,32]. Therefore, we examined whether direct manipulation of F-actin could induce dedifferentiation. Treatment with a Rho/Rac/Cdc42 activator, even in the absence of laminin-332 coating, induced a level of dedifferentiation comparable to that observed with laminin-332 (Fig. 3d). Western blot analysis confirmed increased expression of F-actin, Hippo, and MAPK pathway components, and AP-1 family proteins in dedifferentiated cells, with c-JUN showing a particularly strong upregulation (558%) (Extended Data Fig. 9).

The central role of c-JUN in melanocyte dedifferentiation was confirmed by inhibitor studies. Inhibition of c-JUN using SP600125 effectively blocked dedifferentiation induced by both Rho/Rac/Cdc42 and YAP activation (Fig. 3d, g). Furthermore, the application of specific MAPK inhibitors confirmed the critical role for this signaling cascade in dedifferentiation, as both BRAF and MEK inhibitors effectively prevented dedifferentiation (Fig. 3e, h). Analysis of downstream MAPK branches revealed that JNK inhibition most effectively impeded laminin-332-induced dedifferentiation, followed by ERK inhibition, whereas p38 inhibition had no appreciable effect (Fig. 3e, h). Transcription factor analyses from previous studies demonstrated that ERK predominantly targets c-FOS, STAT, ELK, and c-JUN; JNK mainly regulates c-JUN, CREB, ATF2, SP1, and c-MYC; and p38 primarily affects CREB, ATF2, SP1, and c-MYC[33]. It suggests that the ability of ERK and JNK to modulate c-JUN may be crucial for dedifferentiation, the lack of c-JUN

regulation by p38 likely accounts for its minimal effect on the dedifferentiation.

Considering that canonical Wnt signaling is a key regulator of melanocyte differentiation[29], and that β-catenin knockdown did not affect dedifferentiation (Fig. 3c, f), we explored the role of non-canonical Wnt signaling. Treatment with WNT5A induced a modest degree of melanocyte dedifferentiation (Extended Data Fig. 10a), We also assessed several factors associated with vitiligo, including inflammatory cytokines (TNFα, IFNβ, IFNγ, IL1β, and IL6)[34], oxidative stress (H_2O_2)[35], and rhododendrol, a compound known to induce vitiligo-like depigmentation in humans and animals[36]. Although these factors induced melanocyte dedifferentiation, their effects were less pronounced than those induced by laminin-332 (Extended Data Fig. 10a), suggesting that multiple factors can trigger melanocyte dedifferentiation with varying potencies.

Interestingly, several JAK inhibitors (Ruxolitinib, Delgocitinib, Baricitinib, Abrocitinib, Tofacitinib) significantly suppressed laminin-332-induced dedifferentiation (Extended Data Fig. 10b), indicating a previously unrecognized mechanism by which these agents may promote melanocyte differentiation independent of their immunomodulatory actions. Based on our earlier observation that the EGFR inhibitor Gefitinib showed therapeutic potential in vitiligo animal models[37], we also investigated whether tyrosine kinase inhibitors could directly modulate melanocyte differentiation. Inhibitors targeting EGFR, VEGFR2, IGF1R, c-Kit, Tie2, c-RET, and ALK effectively suppressed dedifferentiation, with particularly strong effects observed for inhibitors of EGFR, IGF1R, c-RET, and ALK (Extended Data Fig. 11).

In summary, our results demonstrates that laminin-332-induced melanocyte dedifferentiation is mediated by an integrin α3β1-RHO-F-actin-Hippo/MAPK-c-JUN signaling axis, with additional modulation by WNT5A, tyrosine kinase, reactive oxygen species, and cytokines (Extended Data Fig. 12). These molecular insights not only advance our understanding of melanocyte dedifferentiation but also highlight multiple therapeutic targets for preventing or reversing this process in vitiligo.

RHO/Hippo/MAPK signaling pathways control melanocyte fate

To confirm the functional significance of the signaling pathways identified in Fig. 3 and Extended Data

Fig. 12, we examined the effects of RHO, Hippo, and MAPK pathway modulators across three experimental systems: cultured melanocytes (Fig. 4a), K14-Kitl transgenic mice (Fig. 4b, c, d), and human skin explants (Fig. 4e, f).

In cultured melanocytes exposed to laminin-332, approximately 50% of cells maintained a mature phenotype (Melan-A positive). Addition of RHO, YAP, or JNK inhibitors increased mature melanocyte proportions to nearly 100%, effectively eliminating dedifferentiated cells (phalloidin single-positive) (Fig. 4a). Conversely, pathway activators substantially reduced mature melanocyte populations, promoting widespread conversion to a dedifferentiated state (Fig. 4a). These observations indicate that inhibition of RHO/YAP/JNK signaling promotes melanocyte differentiation, while pathway activation drives dedifferentiation, supporting our mechanistic findings in Fig. 3.

In K14-Kitl transgenic mice, a well-established model that uniquely harbors melanocytes in the epidermis, topical application of RHO/YAP/JNK inhibitors for two weeks enhanced epidermal pigmentation, as observed by bright-field microscopy (Fig. 4b). Immunofluorescence analysis revealed increased numbers of mature melanocytes, identified by TRP1 and c-Kit co-expression in the basal epidermal layer (Fig. 4c, d). In contrast, four-week treatment with pathway activators caused notable hypopigmentation and accumulation of undifferentiated melanocytes (c-Kit positive/TRP1 negative cells) (Fig. 4b, c, d), confirming the role of these pathways in regulating melanocyte differentiation in vivo.

In human skin explants from healthy donors, treatment with RHO/YAP/JNK inhibitors for one week increased functional melanocytes in the basal layer, evidenced by increased DOPA positive cells (Fig. 4e) and increased Melan-A-positive cell populations (Fig. 4f). Treatment with pathway activators produced opposite effects, reducing both DOPA-positive and Melan-A-positive melanocytes (Fig. 4f), validating these regulatory mechanisms in human skin tissue.

Together, these findings demonstrate that RHO/Hippo/MAPK pathways regulate melanocyte differentiation in opposite directions across in vitro, in vivo, and ex vivo systems, ultimately determining skin pigmentation. The consistency of these results across diverse experimental models highlights the

fundamental importance of these pathways in melanocyte biology.

Melanocyte dedifferentiation in vitiligo patients

Based on our previous findings that vitiligo melanocytes directly contact with laminin-332 (Fig. 1), we sought to determine whether the laminin-332-induced mechanism of melanocyte dedifferentiation, as observed in our *in vitro* studies, is also present in the skin of vitiligo patients.

We first examined melanocyte phenotypes in perilesional skin samples using DOPA reaction analysis. In perilesional vitiliginous skin, melanocytes exhibited markedly reduced DOPA positivity compared with normal controls (Fig. 5a), indicating a substantial loss of melanin synthesis capacity. To identify reliable markers for dedifferentiated melanocytes in patient samples, we evaluated markers previously validated in our *in vitro* studies (Extended Data Fig. 6, 7). Although c-Kit and NGFR were undetectable in perilesional melanocytes (Extended Data Fig. 13a), the combined assessment of DCT/SOX9 and MELAN-A reliably identified dedifferentiating cells. Specifically, dedifferentiated melanocytes were characterized either by a DCT-positive/MELAN-A-negative phenotype or by concurrent SOX9/MELAN-A expression (Fig. 5a). Some cells also demonstrated strong F-actin and p-c-Jun immunoreactivity, consistent with the activation of dedifferentiation-associated signaling pathways identified *in vitro* (Fig. 3, Extended Data Fig. 12).

Previous studies have shown that SOX9 is highly expressed in melanoblasts and is subsequently downregulated during differentiation[38]. Moreover, SOX9 is known to antagonize SOX10[39]-a key promoter of melanocyte differentiation through MITF regulation[40], and plays a critical role in determining melanocyte precursor fate within the hair follicle niche[41]. Elevated SOX9 expression has also been reported in vitiliginous melanocytes[42]. To directly assess the impact of SOX9 on melanocyte phenotype, we overexpressed SOX9 in cultured melanocytes using a pEBMulti episomal expression vector system. Control melanocytes transfected with the empty vector exhibited no detectable expression of SOX9 or the His-tag (Fig. 5b). In contrast, melanocytes transfected with the SOX9 overexpression vector, as confirmed by double-positive staining for SOX9 and the His-tag, showed a marked loss of MELAN-A expression (Fig. 5b), indicating that SOX9

expression suppresses the mature melanocyte phenotype. To further evaluate the role of SOX9 in dedifferentiation, we conducted siRNA-mediated knockdown experiments under laminin-332-induced conditions. Melanocytes transfected with control (MOCK) siRNA and exposed to laminin-332 displayed dedifferentiation features-defined by the presence of SOX9 or absence of MELAN-A-in approximately 50% of cells (Fig. 5c). In contrast, the knockdown of SOX9 (siSOX9) resulted in an almost complete ablation of SOX9-positive cells and a marked increase in the proportion of MELAN-A-positive cells (Fig. 5c), demonstrating that SOX9 depletion prevents laminin-332-induced melanocyte dedifferentiation. Additionally, c-JUN has been reported to induce SOX9 expression[43]. Taken together, these findings suggest that melanocyte dedifferentiation may ultimately be mediated through SOX9-dependent phenotypic changes.

Spatial transcriptome analysis of perilesional vitiliginous skin provided further molecular evidence for melanocyte dedifferentiation. Dedifferentiated/dedifferentiating melanocytes exhibited coordinated upregulation of genes associated with stemness (e.g. SOX9, NGFR, YY1, POU2F1, SOX4, LRIG1), cytoskeleton organization (e.g. RHOC, ACTB, RHOV), Hippo pathway components (e.g. CCN5, CCN1, YAP1), AP-1 family members (e.g. JUN, JUNB, ATF7, JUND), and multiple MAPK pathway constituents (e.g. MAPK9, MAP3K13, MAP3K2, MAPK13) (Fig. 5d). In contrast, differentiated melanocytes predominantly expressed melanogenic genes such as TYRP1, MLANA, TYR, and MITF (Fig. 5d). The expression profiles observed in patient samples were highly consistent with those identified in our *in vitro* studies.

Moreover, histological examination revealed that dedifferentiated melanocytes, as defined by either the DCT-positive/MELAN-A-negative or SOX9/MELAN-A double-positive staining patterns, frequently detached from the BM and migrated toward the outer epidermis or dermis (Extended Data Fig. 13b, c). This cellular instability was further corroborated in three-dimensional skin models, wherein melanoblasts exhibited an inability to maintain stable epidermal residency (Extended Data Fig. 14a-c). Collectively, these results suggest that therapeutic strategies for vitiligo should concurrently address the restoration of melanocyte differentiation and the reinforcement of their retention within the epidermis.

Pharmacological inhibition of melanocyte dedifferentiation demonstrates therapeutic efficacy in multiple vitiligo models

After identifying melanocyte dedifferentiation in vitiligo patients, we investigated whether inhibiting this process could provide therapeutic benefit. We evaluated dedifferentiation inhibitors across multiple experimental systems to assess their efficacy.

We first developed a three-dimensional (3D) skin model that allows precise control of the melanocyte microenvironment. Application of laminin-332 to the transmembrane region induced concentration-dependent depigmentation (Fig. 6a) and created sharply defined areas of pigment loss (Fig. 6b), mimicking the characteristic depigmentation patterns observed in vitiligo lesions. Histological examination revealed that laminin-332 treatment significantly reduced TRP1-positive mature melanocytes (Fig. 6c) while increasing DCT-single-positive dedifferentiating melanocytes (Extended Data Fig. 17b), confirming the induction of melanocyte dedifferentiation. Treatment with the JNK inhibitor SP600125 effectively reversed these changes, restoring pigmentation and increasing mature melanocyte numbers (Fig. 6c).

To validate these observations *in vivo*, we employed a rhododendrol-induced depigmentation model, which has been reported to induce progressive depigmentation in both humans and animals[36]. In K14-Kitl mice, rhododendrol treatment caused substantial depigmentation of both fur and skin (Extended Data Fig. 15a) and induced melanocyte dedifferentiation, most prominent at 10% rhododendrol concentration (Extended Data Fig. 15b). In this model, both cytochalasin D (an actin inhibitor) and SP600125 (a JNK inhibitor) significantly restored pigmentation and increased epidermal TRP1-positive melanocytes (Fig. 6d).

We extended these findings to human tissue by examining *ex vivo* cultured perilesional vitiliginous skin explants. One week of SP600125 treatment significantly increased epidermal MELAN-A-positive melanocytes compared to untreated controls (Fig. 6e). Detailed analysis showed that untreated perilesional skin contained numerous DCT-single-positive dedifferentiating melanocytes, which converted to MELAN-A-positive mature melanocytes following SP600125 treatment (Extended Data Fig. 16b), demonstrating that pharmacological intervention can reverse the dedifferentiated state.

Together, these findings show that dedifferentiation inhibitors effectively restore pigmentation and increase mature melanocyte numbers across diverse experimental systems. The consistent efficacy in three-dimensional skin models, mouse models, and patient-derived skin explants provides compelling evidence that targeting melanocyte dedifferentiation represents a promising therapeutic approach for vitiligo. These results establish both the pathogenic role of melanocyte dedifferentiation in vitiligo and the therapeutic potential of its pharmacological inhibition (Fig. 6f).

Discussion

In the present study, we elucidate a novel mechanism underlying melanocyte loss in vitiligo. Rather than complete cell loss, melanocytes in lesional vitiligo skin undergo dedifferentiation. This phenomenon appears to be initiated by disrupted basement membrane interactions and alterations in the extracellular matrix microenvironment, as documented in our previous observations[14]. Importantly, our findings indicate that this dedifferentiation is regulated by previously unrecognized molecular pathways, thereby providing multiple potential targets for therapeutic intervention.

In the present study, we discovered that manipulation of culture plate with laminin-332 coating induced unexpected melanocyte dedifferentiation *in vitro*. Notably, in healthy skin, the localized absence of laminin-332 surrounding melanocytes contributes to the formation of a unique niche microenvironment. This observation prompted us to hypothesize that melanocyte cell surface proteases may selectively degrade the extracellular matrix, thereby establishing this laminin-332-deficient niche. Supporting this hypothesis, our investigation of membrane-type matrix metalloproteinases (MT-MMPs) in healthy skin revealed that normal epidermal melanocytes expressed markedly high expression levels of both MT1-MMP and MT4-MMP (Extended Data Fig. 18a) which was further confirmed using multiple skin cell lines (Extended Data Fig. 18b) and was also observed in both cultured mature melanocytes and melanoblasts (Extended Data Fig. 18c). Functional analyses further demonstrated that melanocytes actively degraded laminin-332, creating clear zones around the cells, and that knockdown of either MT1-MMP or MT4-MMP significantly attenuated this degradation (Extended Data Fig. 18d). These findings suggest the critical roles of these enzymes in mediating laminin-332 degradation within the melanocyte microenvironment. In perilesional skin from patients with vitiligo, epidermal melanocytes exhibited reduced MT4-MMP expression (Extended Data Fig. 19a), which was associated with abnormal accumulation of laminin-332, while MT1-MMP levels remained largely unchanged (Extended Data Fig. 19b). The mechanism underlying the reduced expression of MT4-MMP in vitiligo melanocytes remains to be elucidated. Moreover, we found that mouse melanocytes lacked

expression of both MT1-MMP and MT4-MMP (Extended Data Fig. 19c), suggesting fundamental species-specific differences in melanocyte biology that are critical to consider in translational research.

We found that in healthy skin, epidermal melanocytes primarily adhere to the basement membrane *via* dystroglycan-laminin-211 interactions. In contrast, vitiligo melanocytes exhibited weakened dystroglycan–laminin-211 binding, which correlates with reduced dystroglycan expression in lesional melanocytes (Extended Data Fig. 20a). Given that dystroglycan is a known substrate of MMP2[44], and our previous observations of elevated MMP2 levels in vitiligo patients[14], this reduction may result from enhanced proteolytic degradation by MMP2. Moreover, laminin-332-induced dedifferentiation was found to decrease dystroglycan expression in melanocytes (Extended Data Fig. 20b), suggesting a potential feedback loop. Reduced dystroglycan weakens the binding affinity to laminin-211, triggering compensatory interactions with laminin-332 that induce dedifferentiation, which in turn further reduces dystroglycan levels. Notably, this study provides the first evidence identifying dystroglycan as the primary adhesion receptor for laminin-211 in melanocytes. Consistent with our observations, melanocyte detachment from the basement membrane has also been reported in patients with congenital muscular dystrophy (CMD) caused by defective dystroglycan-laminin-211 binding[45]. However, these CMD patients do not exhibit vitiligo-like depigmentation, potentially because the detached melanocytes lack exposure to laminin-332 or other associated signals required for initiating dedifferentiation. Finally, considering the established role of dystroglycan in CMD, particularly in dystroglycanopathies affecting on muscle and neural systems[46], and the neural crest origin of melanocytes[47], our findings may offer novel insights and suggest that melanocytes could serve as a readily accessible model for studying CMD-related neural abnormalities.

Based on the aforementioned data, we demonstrated that the maintenance of the laminin-332-deficient niche was regulated by multiple factors. Decreased expression or functional abnormalities of MT1/4-MMP in melanocytes diminished their ability to degrade laminin-332, thereby destabilizing this specialized niche. Moreover, other laminin-332-degrading enzymes, including MMP2, MMP9, MMP3, MMP14, neutrophil elastase, cathepsin G, plasmin, and others, may release laminin-332 fragments that accumulate around

melanocytes and further disrupt niche integrity. In vitiligo, we observed a significant reduction in MT4-MMP expression in melanocytes (Extended Data Fig. 19), coupled with an enrichment of MMP2 near the basement membrane[13]. These concurrent alterations may accelerate the damage to the laminin-332-deficient niche, ultimately promoting melanocyte dedifferentiation in vitiligo. Furthermore, considering that MT-MMPs is crucial for MMP2 activation[48], therapeutic modulation of the dynamic balance between MT-MMPs and MMP2 may represent an important strategy for vitiligo treatment. Additionally, further investigation is warranted to determine whether similar melanocyte alterations occur in conditions characterized by elevated MMP2 levels, such as scarring, chronic eczema, and scleroderma.

In healthy individuals, the relationship between dystroglycan expression in melanocytes and the formation of the epidermal melanocyte network still remains elucidated. We investigated this association and observed that both melanocytes and melanoblasts expressed dystroglycan, with particularly strong expression in melanoblasts (Extended Data Fig. 21a). It is generally accepted that melanocytes originate from the hair follicle bulge, eventually migrate and localize to the niche in the epidermis. Accordingly, our analysis of the perifollicular melanocyte population in healthy skin revealed that mature melanocytes, identified by strong Melan-A positivity, exhibited high dystroglycan expression concomitant with a specific absence of laminin-332. Similarly, immature melanocytes, characterized by weak Melan-A positivity, also exhibited high dystroglycan expression alongside a specific loss of laminin-332 (Extended Data Fig. 21b). These findings suggest that an MT4-MMP-mediated process establishes a laminin-332-deficient microenvironment during the early stages of melanocyte differentiation, ultimately facilitating cellular maturation through the interaction of dystroglycan with laminin-211.

The phenotype switching in melanocyte dedifferentiation identified in this study has significant implications for understanding vitiligo pathogenesis. Previous studies have documented that dedifferentiated melanocytes exhibit a characteristic flattened morphology in cultured vitiliginous melanocytes[49-51]. Furthermore, flattened melanocytes isolated from depigmented epidermis have been shown to revert to a mature, functional state following the removal of hydrogen peroxide[52]. Taken together, these findings provide

strong molecular evidence that melanocytes in lesional vitiligo skin are not completely absent but rather exist in an undifferentiated state. Although we identified several markers, such as c-Kit, DCT, NGFR, SOX9, for detecting dedifferentiating melanocytes, the variability in their expression and the presence of fully dedifferentiated, marker-negative cells indicate that further investigation is warranted to identify more universal markers for reliably detecting residual reprogrammed cells in vitiligo lesions.

Our present data revealed that melanocyte reprograming toward dedifferentiation was mediated by the integrin-α3β1-RHO-F-actin-Hippo/MAPK-c-JUN signaling upon Lamin 332 binding. Notably, treatment with the JNK inhibitor SP600125 effectively reversed this dedifferentiation program, promoting redifferentiation and restoration of the normal melanocyte phenotype. Although inhibitors targeting RHO, YAP, and JNK pathways showed efficacy in our models, these agents are currently used predominantly in oncology, warranting the development of more suitable compounds for vitiligo therapy. Interestingly, we observed that JAK inhibitors enhanced melanocyte differentiation independent of their immunomodulatory effects, possibly through STAT3-mediated regulation of c-JUN/c-FOS[53]. This mechanism further supports the clinical application of JAK inhibitors, although more selective agents targeting the dedifferentiation pathway may offer promising therapeutic potential in the future.

Cellular dedifferentiation, a process in which specialized cells revert to a less differentiated state, has been extensively studied in cultured cells, particularly in induced pluripotent stem cells (iPSCs)[54]. However, in human tissues, dedifferentiation occurs only under limited and extreme pathological conditions, such as severe liver or neural injury[55,56]. In studies of ocular lineage differentiation from iPSCs, laminin-211 has been shown to direct differentiation toward the neural crest lineage, whereas laminin-332 directs differentiation toward the epithelial lineage[57]. These observations suggest that laminin-211 is critical for maintaining neural crest-derived cell properties, while interactions with laminin-332 disrupts this homeostasis and forces mature melanocytes to undergo reprogramming, a phenomenon consistent with our experimental findings (Fig. 2). Furthermore, transgenic mice engineered to express laminin-211 in the epidermal basement membrane exhibit a human-like distribution of melanocytes in the basal layer[58], indicating the essential role of laminin-

211 in melanocyte localization in mice. Conversely, the absence of epidermal melanocytes in the dorsal skin of C57BL/6 mice may be attributed to insufficient expression of laminin-211 (Extended Data Fig. 22a), which was found to be important for maintaining the differentiated state of melanocytes in the present study. Furthermore, the outer side of C57BL/6 mouse ears exhibits significantly higher pigmentation compared to the corresponding inner side, a pattern that coincides with laminin-211 expression distribution (Extended Data Fig. 22b). These findings demonstrate a strong correlation between laminin-211 and melanocyte distribution. Further investigation into this relationship may elucidate the mechanisms underlying the differential pigmentation patterns observed across various anatomical regions in mammals.

Our study revealed that the pathological microenvironment in vitiligo could trigger melanocyte dedifferentiation through RHO-F-actin-dependent activation of Hippo and MAPK pathways, converging on c-JUN signaling (Fig. 3). Notably, Hippo signaling has been reported to regulate epithelial tissue reprogramming[59] and to control MITF expression in neural crest cells in cooperation with PAX3, thereby determining melanocyte fate specification[60]. In the present study, the identification of this mechanism not only provides therapeutic opportunities for vitiligo treatment (Fig. 6) but also demonstrates the potential for controlled manipulation of skin pigmentation in normal tissue (Fig. 4), suggesting promising applications in clinical pigmentation management.

Beyond the core signaling pathways identified in the present study, our data also indicated other multiple factors, including WNT5A, tyrosine kinases, ROS, various cytokines, also played a role in melanocyte differentiation (Extended Data Fig. 12). These findings indicate the importance of comprehensively addressing the local microenvironment. Although individual inflammatory cytokines induce modest dedifferentiation, their combined effects *in vivo* may be considerably greater. Moreover, the transient epidermal residency of dedifferentiated melanocytes (Extended Data Fig. 13) suggests that effective treatment strategies for vitiligo might require a dual approach: combining agents that promote differentiation with interventions designed to melanocyte migration and retention, such as UVB phototherapy[61] or minimally invasive treatments that stimulate melanocyte recruitment[62].

These findings represent a significant advancement in our understanding of vitiligo pathogenesis and indicate promising new therapeutic strategies. Future research should prioritize the development of more specific markers for dedifferentiated melanocytes, the refinement of targeted therapies, and the exploration of approaches to enhance melanocyte retention within the epidermis. Recognizing melanocyte dedifferentiation as a key pathogenic mechanism opens promising new avenues for therapeutic intervention in this challenging disease.

Methods

Human skin specimens

Frozen biopsies were obtained from lesional and perilesional skin of well-defined patients with nonsegmental vitiligo (n = 15, ten patients in a progressive state and five patients in a stable state) (Supplementary Table 1) and from corresponding sites on healthy donors (n = 7). The progressive state of vitiligo was defined by the development of new lesions or the extension of pre-existing lesions in the previous 6 months, and the stable state was defined by no increase in the size of existing lesions and an absence of new lesions in the previous year. Written informed consent was obtained from all participants prior to study inclusion. The study was approved by the Medical Ethics Committee of Osaka Metropolitan University (No. 4152). All procedures involving human subjects were in accordance with the Helsinki Declaration of 1975, as revised in 1983.

Cell Culture

Primary human melanocytes, including HEMn-DP (#C2025C, Thermo Fisher Scientific, Waltham, USA), HEMn-MP (#C1025C, Thermo Fisher Scientific Inc.), and other human epidermal melanocytes (#LMC/#LC1C1022/#M4C0760) obtained from Kurabo Co. (Osaka, Japan), were cultured in medium 254 (Cascade Biologics^{TM}, Invitrogen, CA, USA). Melanoblasts (36011-12, Celprogen, CA, USA) were maintained in Human Melanoblast Stem Cell Media (#M36011-12, Celprogen) using pre-coated flasks (#E36011-12-T75, Celprogen). All cell lines were incubated at 37°C in a humidified atmosphere containing 5% CO2. For laminin coating experiments, culture plates were treated overnight at 4°C with either 20μg/ml laminin-211 (#BLA-LN211-02, BioLamina, Sundbyberg, Sweden) or 20μg/ml laminin-332 (#BLA-LN332-02, BioLamina).

Antibody Neutralization Experiments

Melanocytes were pre-incubated with one of the following antibodies at a final concentration of 10μg/ml for 30 minutes: Rabbit IgG control (#ab172730, Abcam, Cambridge, UK), Mouse IgG control (#ab37355, Abcam), anti-dystroglycan (#ab234587, Abcam), anti-integrin β1 (#PA5-29606, Thermo Fisher Scientific Inc.), and anti-integrin α7 (#ab195959, Abcam). After pretreatment, cells were seeded onto laminin-211-coated coverglass (#C018001, MATSUNAMI GLASS IND., LTD, Osaka, Japan) and incubated for 4-6 hours before evaluating cell adhesion.

Melanin Content Measurement

Harvested cells were solubilized in Solvable solution (6NE9100, Perkin Elmer, Waltham, Massachusetts, USA) at 80°C for 30 min. The melanin content of each sample was then quantified by measuring its absorbance at 405 nm using a spectrophotometer. A standard curve generated with a synthetic melanin standard (M8631, Sigma-Aldrich, St. Louis, USA) was used to calculate the melanin concentration in each sample.

Multi-lineage Differentiation

To assess differentiation potential, laminin-332-treated, dedifferentiated melanocytes were cultured in lineage-specific induction media. For neural differentiation, cells were maintained in Mesenchymal Stem Cell Neurogenic Differentiation Medium (#C-28015, PromoCell, Heidelberg, Germany). For chondrogenic differentiation, the MesenCult-ACF Chondrogenic Differentiation Kit (#ST-05455, Veritastk, Tokyo, Japan) was used. For mesodermal differentiation, cells were cultured in a 1:1 mixture of DMEM (#D5921, Sigma-Aldrich) and F12 (#N4888, Sigma-Aldrich), supplemented with 1× non-essential amino acid solution (#139-15651, FUJIFILM Wako Pure Chemical Corporation, Osaka, Japan), 60 pM TGF-b1 (#240-B-010/CF, R&D Systems, Minneapolis, USA), 10% fetal calf serum (#10270106, Thermo Fisher Scientific Inc.), and 1×

penicillin-streptomycin solution (#168-23191, FUJIFILM Wako Pure Chemical Corporation). Differentiation was evaluated after 1-4 weeks using appropriate lineage-specific markers.

MACS Cell Sorting

C-Kit-positive and c-Kit-negative cell populations were isolated using magnetic-activated cell sorting (MACS). Sorting was performed using a MiniMACS Starting Kit (#130-090-312, Miltenyi Biotec, Bergisch Gladbach, Germany) and a CD117 MicroBead Kit (#130-091-332, Miltenyi Biotec), following the manufacturer's instructions.

3D Skin Model

Three-dimensional skin models containing a dermal compartment were constructed in accordance with our previously established protocol[14]. Briefly, human dermal fibroblasts were embedded in an acidic collagen solution (KKN-IAC-50, Koken Co. Ltd, Tokyo, Japan). Following a 48-hour gel contraction period, melanocytes or melanoblasts were co-seeded with keratinocytes onto the contracted dermal equivalent. For spatially controlled laminin-332 treatment, specific regions were defined using Culture-Inserts (#80209, ibidi GmbH, Gräfelfing, Germany). After laminin-332 coating and removal of the Culture-Inserts, melanocytes and keratinocytes were co-seeded to form the epidermal layer. These 3D skin models were subsequently maintained at the air-liquid interface for 10 days.

Mouse Experiments

Eight-week-old male K14-Kitl mice (#RBRC00694, RIKEN BioResource Research Center, Tsukuba, Japan) were used for all *in vivo* experiments. Rhododendrol (chemical name: 4-(4-hydroxyphenyl)-2-butanol; trade name Rhododenol®) was generously provided by Kanebo Cosmetics Inc. (Tokyo, Japan). A stock solution of 20% (w/v) rhododendrol was prepared in a 50:50 (v/v) ethanol/sesame oil mixture as the vehicle. To establish a lukoderma mouse model, animals were treated topically with 100 μL of 20% (w/v) rhododendrol on the dorsal skin once daily for one month. This induction period was followed by a two-

week drug intervention phase. To specifically examine melanocyte dedifferentiation, additional mice received a single topical application of rhododendrol 24 hours before tissue collection and analysis. Specifically, 100 μL of a 5%, 10%, or 15% (w/v) rhododendrol solution was applied to the dorsal skin of each mouse. All animal experiments were conducted in accordance with protocols approved by the Institutional Animal Care and Use Committee (Approval No. 23018).

Immunofluorescence and Immunohistochemistry

Frozen skin sections (6μm thickness) were fixed in 4% paraformaldehyde (163-20145, FUJIFILM Wako Pure Chemical Corporation) for 15 min at room temperature, followed by blocking with 5% bovine serum albumin (BSA) for 30 min. Sections were then incubated with primary antibodies (Supplementary Table 2), diluted 1:100 in blocking solution, overnight at 4 °C. Following primary antibody incubation, sections were washed three times for 5 minutes each with PBS containing 0.05% Tween-20 (161-24801, FUJIFILM Wako Pure Chemical Corporation). Appropriate secondary antibodies (Supplementary Table 3), diluted 1:1,000 in blocking solution, were then applied for 1 hour at room temperature in the dark. Sections were subsequently washed three times with 0.05% Tween-20 in PBS for 5 minutes per wash. Nuclei were counterstained with DAPI (340-07971, FUJIFILM Wako Pure Chemical Corporation). Slides were imaged using an LSM 710 confocal laser scanning microscope (Carl Zeiss AG, Oberkochen, Germany), and images were acquired with ZEN 2012 software (Carl Zeiss AG). Quantification of positively stained cells and mean fluorescence intensity was performed using ImageJ software (National Institutes of Health, http://rsb.info.nih.gov/ij/index.html).

Immuno-electron Microscopy

Skin tissues were fixed in 4% paraformaldehyde (163-20145, FUJIFILM Wako Pure Chemical Corporation) for 30 min at room temperature, followed by three washes in PBS (5 min each). Tissues were were then cryoprotected by immersion in 30% sucrose at 4 °C overnight, and subsequently embedded in OCT compound (#45833, Funakoshi Corporation, Tokyo, Japan). Frozen sections (7μm thick) were prepared

and permeabilized in 0.25% saponin (47036, MilliporeSigma, Burlington, Massachusetts, USA) for 30 min. Sections were blocked for 30 min in PBS containing 0.1% saponin, 10% BSA (014-15151, FUJIFILM Wako Pure Chemical Corporation), 10% normal goat serum (16210072, Thermo Fisher Scientific), and 0.1% gelatin from coldwater fish skin (G7041, MilliporeSigma). Samples were then incubated with the primary antibody against Laminin α3 (#FDV-0024, Funakoshi) diluted in blocking buffer overnight at 4 °C. Following several washes, the sections were incubated with nanogold-conjugated anti-mouse IgG (1.4 nm in diameter; 1:200; #2003, Nanoprobes, Yaphank, NY, USA) in blocking solution for 2 h at room temperature. The nanogold signal was enhanced using the GoldEnhance EM kit (2113, Nanoprobes) for 4 min at room temperature. Samples were post-fixed in 1% osmium tetroxide (#157-01141, FUJIFILM Wako Pure Chemical Corporation), dehydrated through a graded ethanol series, and embedded in TAAB EPON 812 embedding resin (#342-2, Nisshin EM, Tokyo, Japan). Ultrathin sections (70 nm) were cut, stained with uranyl acetate and lead citrate, and imaged using a Talos F200C G2 transmission electron microscope (Thermo Fisher Scientific) equipped with a CCD-based camera system (Advanced Microscopy Techniques, Woburn, MA, USA).

Proximity Ligation Assay (PLA)

Frozen human skin sections were blocked with Duolink blocking solution (#DUO82007, MilliporeSigma) for 30 min at 37 °C. The sections were then incubated overnight at 4 °C with primary antibodies (diluted 1:100). After this incubation, the sections were washed in Duolink In Situ Wash Buffer A (#DUO82046, MilliporeSigma) and subsequently incubated with Duolink In Situ PLA probes (Mouse PLUS, #DUO92001; Rabbit MINUS, #DUO92005; MilliporeSigma) for 90 min at 37 °C. This was followed by ligation and signal amplification using the Duolink In Situ Detection Reagents Red kit (#DUO92008, MilliporeSigma). For co-staining of melanocytes, an anti-c-kit antibody (#AF332, R&D Systems) was included along with the other primary antibodies during the overnight incubation. During the PLA probe incubation step, a corresponding Alexa Fluor Plus 488-conjugated Donkey anti-Goat IgG (#A32814, Thermo Fisher Scientific) was added to

detect the c-kit primary antibody. This approach allowed the simultaneous visualization of melanocytes in the tissue sections. during the PLA probe incubation step. After a final wash in Duolink In Situ Wash Buffer B (#DUO82049, MilliporeSigma) for 30 min, the sections were mounted with Duolink In Situ Mounting Medium containing DAPI (#DUO82040, MilliporeSigma) to counterstain nuclei. The slides were then examined under an LSM 710 confocal laser scanning microscope (Carl Zeiss AG), and fluorescent images were captured using ZEN 2012 software (Carl Zeiss AG).

RNA Sequencing and Analysis

RNA sequencing and library preparation were performed by Takara Bio Inc. using the SMART-Seq v4 Ultra Low Input RNA protocol. Sequencing was conducted on an Illumina NovaSeq 6000 platform with NovaSeq Control Software v1.7.5, Real Time Analysis (RTA) v3.4.4, bcl2fastq2 v2.20, and DRAGEN Bio-IT Platform v3.9.3. Each experimental group included three biological replicates, with an average sequencing depth of approximately 55.08 million reads per sample. Reads were aligned to the human genome (GRCh38.primary_assembly.genome.fa.gz) using GENCODE annotation (v39; gencode.v39.primary_assembly.annotation.gtf.gz). Differential gene expression analysis was conducted using DESeq2, and gene ontology (GO) enrichment analysis was performed with Srplot[63]. Gene Set Enrichment Analysis (GSEA) was carried out using GSEA v4.3.3 in accordance with the official GSEA User Guide, with gene sets derived from the c2.cp.wikipathways.v2024.1.Hs.symbols collection.

Spatial Transcriptomics

Spatial transcriptomic analysis was performed using the Visium HD Spatial Gene Expression platform (10x Genomics) at the Yamaguchi University Institute of Gene Research. A formalin-fixed, paraffin-embedded (FFPE) skin tissue block from a perilesional area of a non-segmental vitiligo patient was analyzed. From each FFPE block, two consecutive 5 μm sections were cut and directly mounted onto Visium HD capture slides. RNA was extracted from adjacent sections to assess integrity and purity; only samples meeting internal quality thresholds for degradation proceeded to library preparation. After placement, the tissue

sections underwent hematoxylin and eosin (H&E) staining. A 6.5 mm × 6.5 mm capture area containing 2 μm high-density spots was used to spatially profile approximately 18,000 genes at near single-cell resolution. Downstream data processing-including quality control, gene expression mapping, and clustering analysis-was performed using the Loupe Browser (10x Genomics), enabling spatially resolved transcriptomic profiling of the vitiligo skin tissue.

Western Blot Analysis

Protein extraction from cell pellets and the subsequent Western blot analysis were performed as described in our previous study[64]. In each assay, 5 μg of extracted protein was used. Primary antibodies were applied at the dilutions specified in Supplementary Table 4, with the anti-GAPDH antibody serving as the internal loading control. Signal intensities of the immunoreactive bands were quantified using ImageJ densitometry software (National Institutes of Health, http://rsb.info.nih.gov/ij/index.html).

DOPA Reaction

Frozen skin sections were fixed in 1% glutaraldehyde for 1 hour, followed by 2-3 washes with PBS. The sections were then incubated at 37°C for 2 hours in a 0.1% L-DOPA solution (#043-30563, FUJIFILM Wako Pure Chemical Corporation) to facilitate melanin synthesis, as L-DOPA serves as a substrate for tyrosinase activity. After incubation, the sections were washed 2-3 times with PBS and post-fixed with glutaraldehyde (#073-06511, FUJIFILM Wako Pure Chemical Corporation). Subsequently, the sections were washed, dehydrated through an ethanol series, and mounted for microscopic observation.

siRNA Knockdown

Human epidermal melanocytes were transfected with small interfering RNAs (siRNAs) using Lipofectamine RNAiMAX transfection reagent (#13778030, Thermo Fisher Scientific) according to the manufacturer's instructions. Each siRNA was used at a final concentration of 30 nM. Six hours after transfection, the medium was replaced with fresh growth medium. Knockdown efficiency for each target

gene was confirmed by quantitative real-time PCR (qPCR) on extracted RNA. A non-targeting siRNA (siMOCK, #AM4611, Thermo Fisher Scientific) was used as a negative control. Target-specific siRNAs (Thermo Fisher Scientific Silencer Select siRNAs) were used to knock down the following genes listed in Supplementary Table 5. All siRNA reagents were purchased from Thermo Fisher Scientific.

Glycosidase Digestion and Cell Adhesion Assay

Melanocytes were seeded on laminin-211-coated coverglass (#C018001, MATSUNAMI GLASS Ind., Ltd., Osaka, Japan). Glycosidase digestion was performed in OptiMEM medium at 37 °C. To remove O-linked oligosaccharides from α-dystroglycan on the cell surface, cells were first incubated with neuraminidase (0.1-0.5 U/mL, #P0720S, New England Biolabs, Ipswich, MA, USA) for 2 hours. This neuraminidase treatment cleaved terminal sialic acid residues, thereby exposing the underlying O-linked oligosaccharide chains on α-dystroglycan. After the 2-hour incubation, the neuraminidase-containing solution was aspirated, and cells were gently washed with phosphate-buffered saline (PBS). Subsequently, cells were incubated with O-glycosidase (0.05-0.5 U/mL, #P0733S, New England Biolabs) in fresh OptiMEM medium for another 2 hours to remove the exposed oligosaccharides. Controls were treated with OptiMEM containing enzyme buffer alone under identical conditions. Cell adhesion to laminin-211-coated coverslips was evaluated by microscopy 2-6 hours post-treatment.

Overexpression of SOX9 in Human Epidermal Melanocytes

Human epidermal melanocytes were transfected with either a human SOX9-expressing episomal plasmid or an empty vector control. The SOX9 expression vector was a customized pEBMulti-Puro episomal plasmid (FUJIFILM Wako Pure Chemical Corporation) carrying the human SOX9 gene. Transfections were performed using the Neon™ NxT Electroporation System (#N1096, Thermo Fisher Scientific) according to the manufacturer's instructions. Each transfection reaction contained 2 µg of episomal vector DNA mixed with Lipofectamine™ LTX transfection reagent (#15338030, Thermo Fisher Scientific). At 24, 48 and 72 hours post-transfection, cells were fixed for immunofluorescence analysis to assess SOX9 overexpression.

Fixed cells were incubated with primary rabbit antibodies against SOX9 (rabbit anti-SOX9, #AB5535, Sigma-Aldrich), Melan-A (mouse IgG2b anti-Melan-A, #SIG-38160, BioLegend, San Diego, CA, USA), and the His-tag (mouse IgG1 anti-His-tag, #12698, Cell Signaling Technology). The stained samples were then examined by fluorescence microscopy. The presence of robust nuclear SOX9 immunoreactivity and positive His-tag staining, indicated successful overexpression of the SOX9 transgene in the transfected melanocytes.

Ex Vivo Culture of Human Skin Explants

Full-thickness human skin explants were obtained from healthy donors and vitiligo patients after obtaining informed consent. For experiments involving healthy skin (Fig. 4), tissues were collected from three independent donors. Each donor's tissue was divided into multiple small explants, and each drug treatment condition was assessed with three biological replicates (n = 3 per condition). For vitiligo skin (Fig. 6), a total of four 4-mm punch biopsies (two biopsies per patient) were obtained from the edge of lesional areas from two patients. Each biopsy was bisected, generating paired control and drug-treated samples, resulting in four biological replicates for each treatment condition (n = 4 per condition). Healthy donor and vitiligo patient explants were cultured and analyzed separately. Each skin explant was placed on a cell culture insert (8 μm pore size, #141082, Thermo Fisher Scientific) with the dermal side in contact with the culture medium and the epidermal side exposed to air. The culture medium consisted of Dulbecco's Modified Eagle Medium (DMEM, #044-29765, FUJIFILM Wako Pure Chemical Corporation) supplemented with 10% fetal bovine serum (FBS, #10270106, Thermo Fisher Scientifi) and 1× penicillin-streptomycin solution (PS, #168-23191, FUJIFILM Wako Pure Chemical Corporation). Explants were maintained at 37 °C in a humidified 5% CO_2 incubator for 7 days, a duration well within the viability window reported for ex vivo human skin cultures. The culture medium was refreshed every two days. Drug treatments were administered by adding test compounds directly to the culture medium. Treatments were applied at the time of medium change to ensure

consistent exposure, and the vehicle control consisted of an equivalent volume of dimethyl sulfoxide (DMSO) in the medium.

Drug Treatment Methods

For in vitro experiments, cells were cultured in Medium 254 and treated for 24-48 hours with various compounds dissolved in DMSO. Control cells received an equivalent volume of DMSO as a vehicle control. Prior to these treatments, each compound underwent dose-response assays using serial dilutions to determine the highest concentration that was both non-toxic and effective. The optimal concentrations identified were used in all subsequent experiments and are detailed in Supplementary Table 6.

For in vivo experiments, compounds were dissolved in a 50:50 (v/v) ethanol/sesame oil mixture and topically applied daily to the dorsal skin of KRT14-Kitl mice for two weeks. Control mice received the vehicle solution without compound. Dose–response assays were conducted beforehand to establish the highest non-toxic and effective concentrations, which were then employed in all experiments. The final working concentrations are listed in Supplementary Table 7.

For ex vivo experiments, skin explants were maintained for one week in DMEM supplemented with 10% FBS and 1% penicillin-streptomycin (PS). The culture medium, containing the respective compounds or DMSO vehicle, was replaced every two days. Prior dose–response assays determined the optimal non-toxic and effective concentrations for each compound, which were subsequently used in all experiments. These concentrations are provided in Supplementary Table 8.

Statistical Analysis

All experiments were repeated at least three times, and results are presented as the mean ± standard deviation (SD). Statistical analyses were performed using unpaired two-tailed Student's t-tests, one-way analysis of variance (ANOVA) with Dunnett's post hoc test, or two-way ANOVA, as appropriate. The same statistical approach was applied to both in vitro and in vivo data. Statistical significance was defined as $p <$

0.05. All analyses were carried out using GraphPad Prism version 9.5.3 (GraphPad Software, Boston, MA, USA).

Data Availability

The data that support the findings of this study are available from the corresponding author upon reasonable request.

Acknowledgements

We gratefully acknowledge Hideki Nakagawa of the Research Support Platform at Osaka Metropolitan University Graduate School of Medicine for providing expert technical assistance with electron microscopy.

Figure legend

Figure 1. Distinct Adhesion Patterns between Normal and Vitiligo Melanocytes. a. Immunofluorescence analysis of laminin distribution in healthy skin and perilesional vitiliginous skin (vitiligo-PL). Laminin-211 (LN211) includes antibodies against laminin alpha 2 chain (LNα2), beta 1 chain (LNβ1), gamma 1 chain (LNγ1); Lamin-332 (LN332) includes antibodies against laminin alpha 3 chain (LNα3), beta 3 chain (LNβ3), gamma 2 chain (LNγ2). White arrow indicates melanocytes. Scale bar: 5 μm. **b**. Immuno-electron microscopy validation of laminin α3 (LNα3) distribution around melanocytes. Scale bar: 1 μm. **c**. Schematic diagram of the proximity ligation assay (PLA) and melanocyte antibody (c-Kit) immunofluorescence co-staining. **d**. Proximity ligation assay analysis of protein interactions in normal and vitiligo melanocytes. The target cell surface proteins on melanocytes (MC) including dystroglycan (DG), integrin β1 (ITGβ1) and Discoidin domain receptor family, member 1 (DDR1). The target matrix proteins on basement membrane (BM) including laminin α2 (LNα2), laminin-332 (LN332), laminin α5 (LNα5) and Collagen IV (Col4). Melanocytes are co-stained with antibody against c-Kit. The Scale bar: 50 μm. **e**. Schematic model of melanocyte-basement membrane adhesion in healthey and perilesional vitiliginous skin. **f**. Validation of dystroglycan-mediated adhesion through antibody neutralization, siRNA knockdown, and glycosidase treatment. Scale bar: 500 μm.

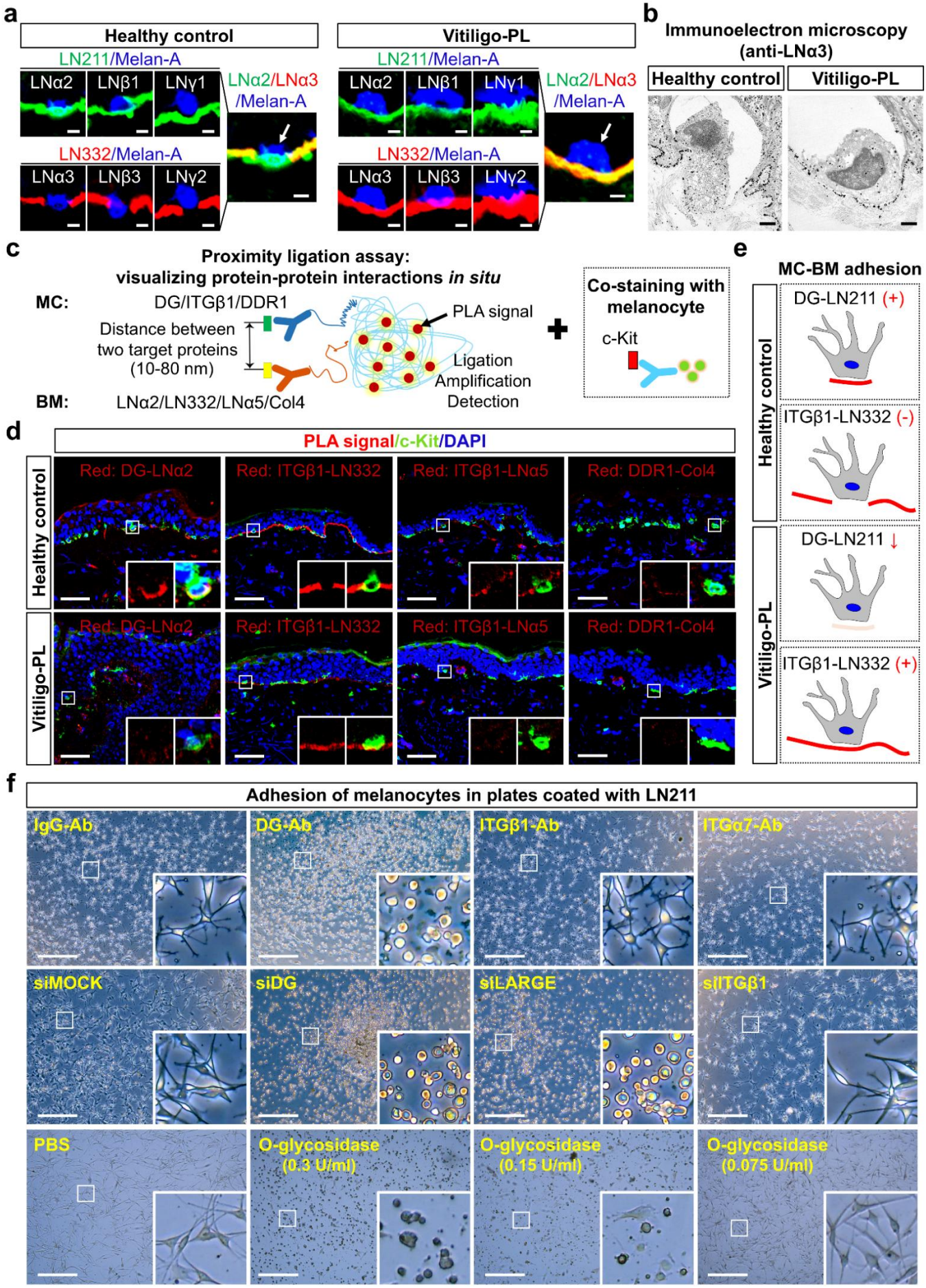
a
Healthy control
Vitiligo-PL
LN211/Melan-A
LNα2
LNβ1
LNγ1
LNα2/LNα3
/Melan-A
LN332/Melan-A
LNα3
LNβ3
LNγ2
b
Immunoelectron microscopy
(anti-LNα3)
Healthy control
Vitiligo-PL
c
Proximity ligation assay:
visualizing protein-protein interactions in situ
MC:
DG/ITGβ1/DDR1
Distance between
two target proteins
(10-80 nm)
PLA signal
Ligation
Amplification
Detection
BM:
LNα2/LN332/LNα5/Col4
Co-staining with
melanocyte
c-Kit
d
PLA signal/c-Kit/DAPI
Healthy control
Vitiligo-PL
Red: DG-LNα2
Red: ITGβ1-LN332
Red: ITGβ1-LNα5
Red: DDR1-Col4
e
MC-BM adhesion
Healthy control
DG-LN211 (+)
ITGβ1-LN332 (-)
Vitiligo-PL
DG-LN211 ↓
ITGβ1-LN332 (+)
f
Adhesion of melanocytes in plates coated with LN211
IgG-Ab
DG-Ab
ITGβ1-Ab
ITGα7-Ab
siMOCK
siDG
siLARGE
siITGβ1
PBS
O-glycosidase
(0.3 U/ml)
O-glycosidase
(0.15 U/ml)
O-glycosidase
(0.075 U/ml)

Figure 2. Laminin-332 Induces Melanocyte Dedifferentiation. a. Morphological and protein expression changes in laminin-332-treated melanocytes. Scale bar: 100 μm **b.** Analysis of melanin content following laminin-332 treatment. *** P<0.001, NS: Not significant. **c.** Analysis of melanogenic protein expression after laminin-332 treatment. Lane 1: control cells treated with LN211. Lane 2: c-Kit-positive cells after laminin-332 treatment. Lane 3: c-Kit-negative cells after laminin-332 treatment. Lower panel shows quantification. ** P<0.01, *** P<0.001, NS: Not significant. **d.** GSEA analysis showing enriched pathways in laminin-332-treated melanocytes. **e.** Multi-lineage differentiation potential of dedifferentiated melanocytes. Neurofilament detection after neural induction, collagen 2 detection after chondrogenic induction, and αSMA detection after myogenic induction. Scale bar: 100 μm.

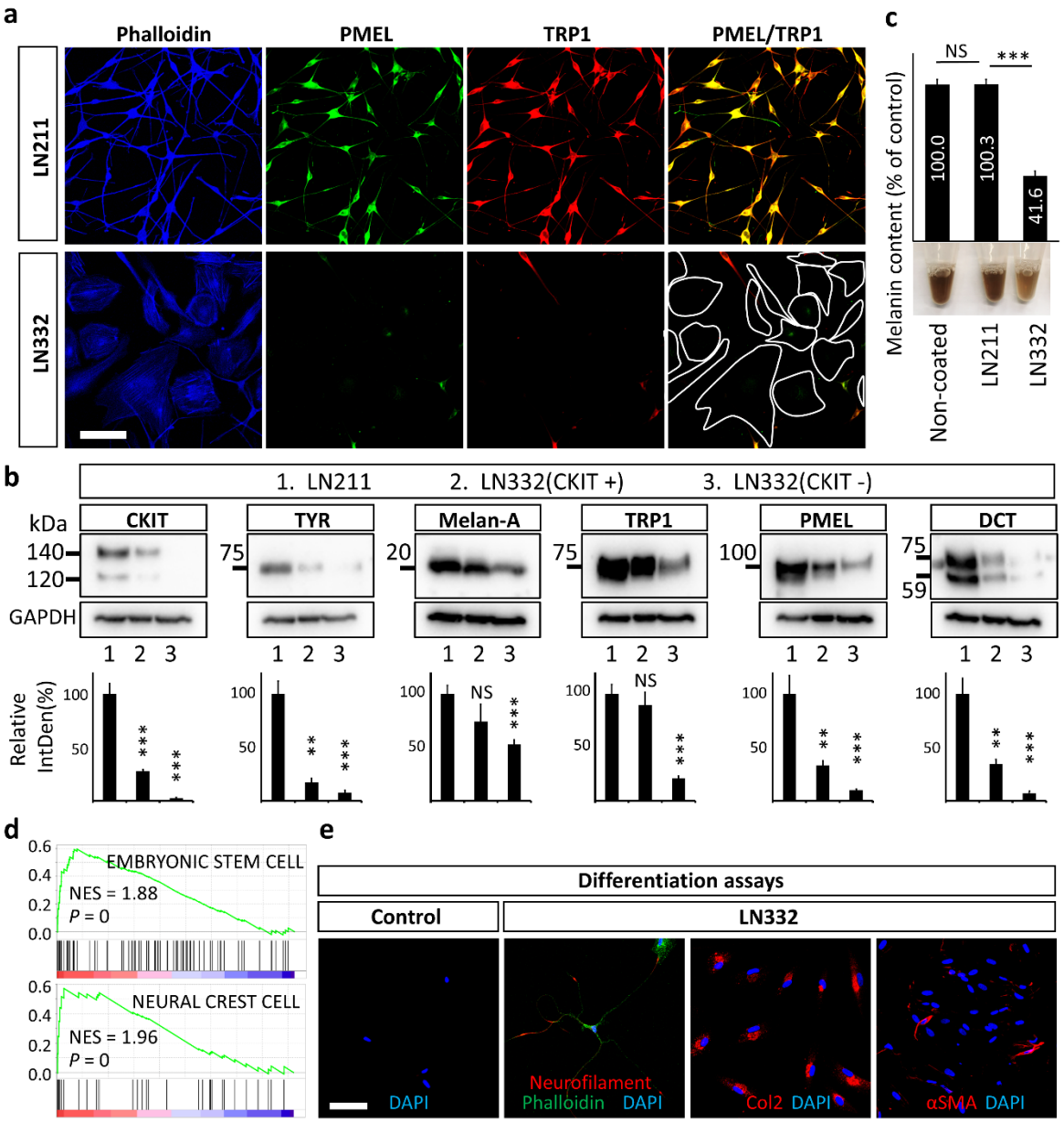

Figure 3. Molecular Mechanisms of Laminin-332-Induced Dedifferentiation. a. RNA-seq analysis of differentially expressed genes. |LogFC|>1 FDR<0.05. **b.** GO enrichment analysis of signaling pathways. |LogFC|>1 FDR<0.05. **c.** Representative images of knockdown experiments. Scale bar: 100 μm **d.** Rescue effects of simultaneous activator and inhibitor treatment. Scale bar: 100 μm. **e.** Effects of different MAPK pathway inhibitors on melanocyte differentiation. Scale bar: 100 μm. **f-h.** Quantification of dedifferentiation rates under various treatments. * P<0.05, ** P<0.01, *** P<0.001, NS: No significance.

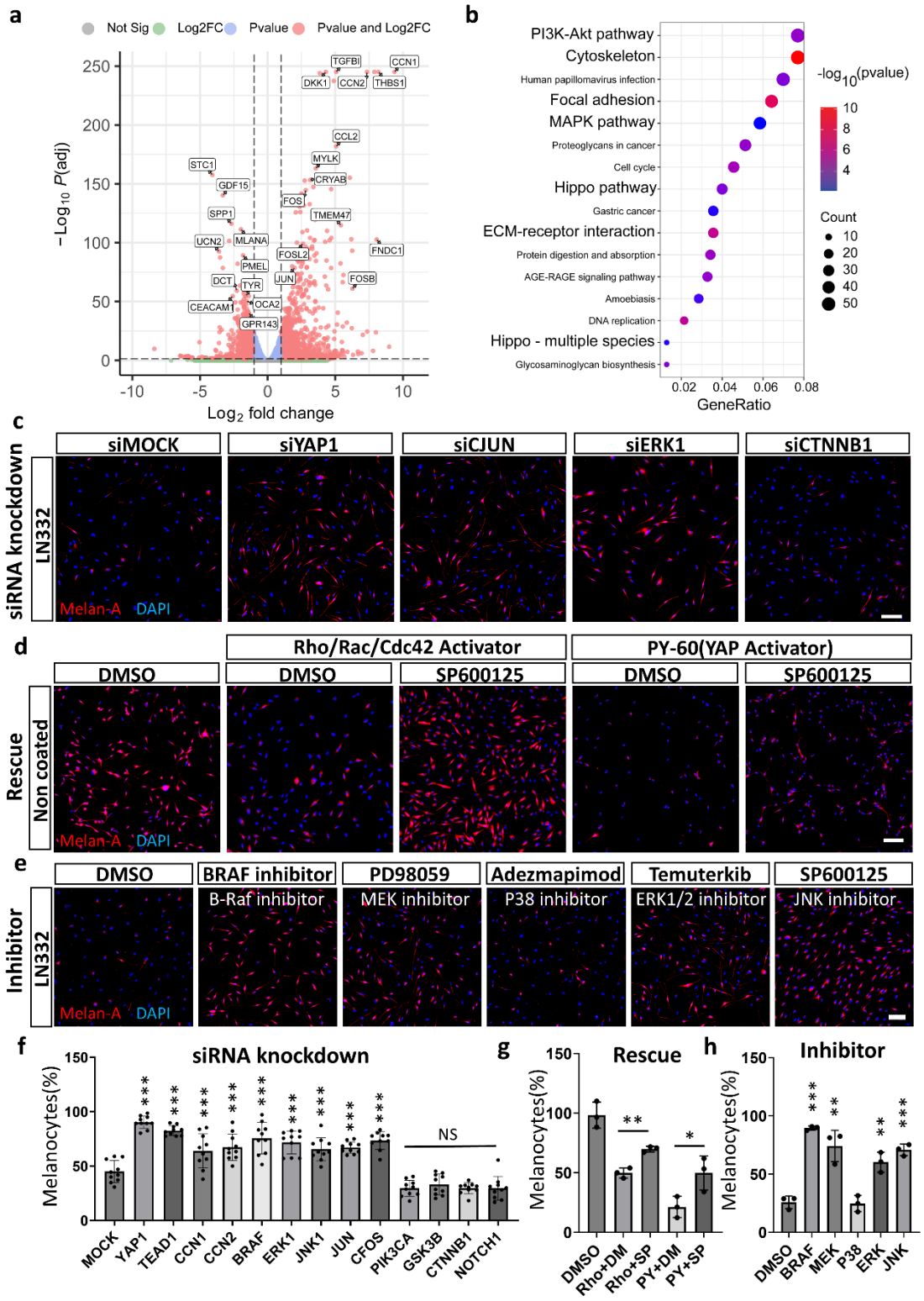

Figure 4. Validation of RHO/Hippo/MAPK Pathway-Directed Melanocyte Differentiation Status Across Multiple Models. **a.** Impact of dedifferentiation pathways on mature melanocyte numbers in cultured cells. red: anti-melan-A, blue: Phalloidin. Scale bar: 100 μm. **b-d.** Effects of dedifferentiation pathways on mature melanocyte numbers and pigmentation phenotype in K14-Kitl mice. **b,** Bright field showing skin pigmentation levels. Scale bar: 100 μm. **c,** Immunofluorescence staining showing mature melanocytes (red: anti-TRP1, blue: anti-collagen 4). **d,** Immunofluorescence staining showing immature melanocytes (green: anti-c-Kit, blue: anti-collagen 4). c-Kit single-positive cells in epidermis represent immature melanocytes. Scale bar: 50 μm. **e-f.** Effects of dedifferentiation pathways on mature melanocyte numbers in human skin explants. **e,** DOPA staining showing distribution of functionally mature melanocytes. Scale bar: 100 μm. **f.** Immunofluorescence staining showing mature melanocytes (red: anti-Melan-A, blue: anti-collagen 4). Scale bar: 50 μm.

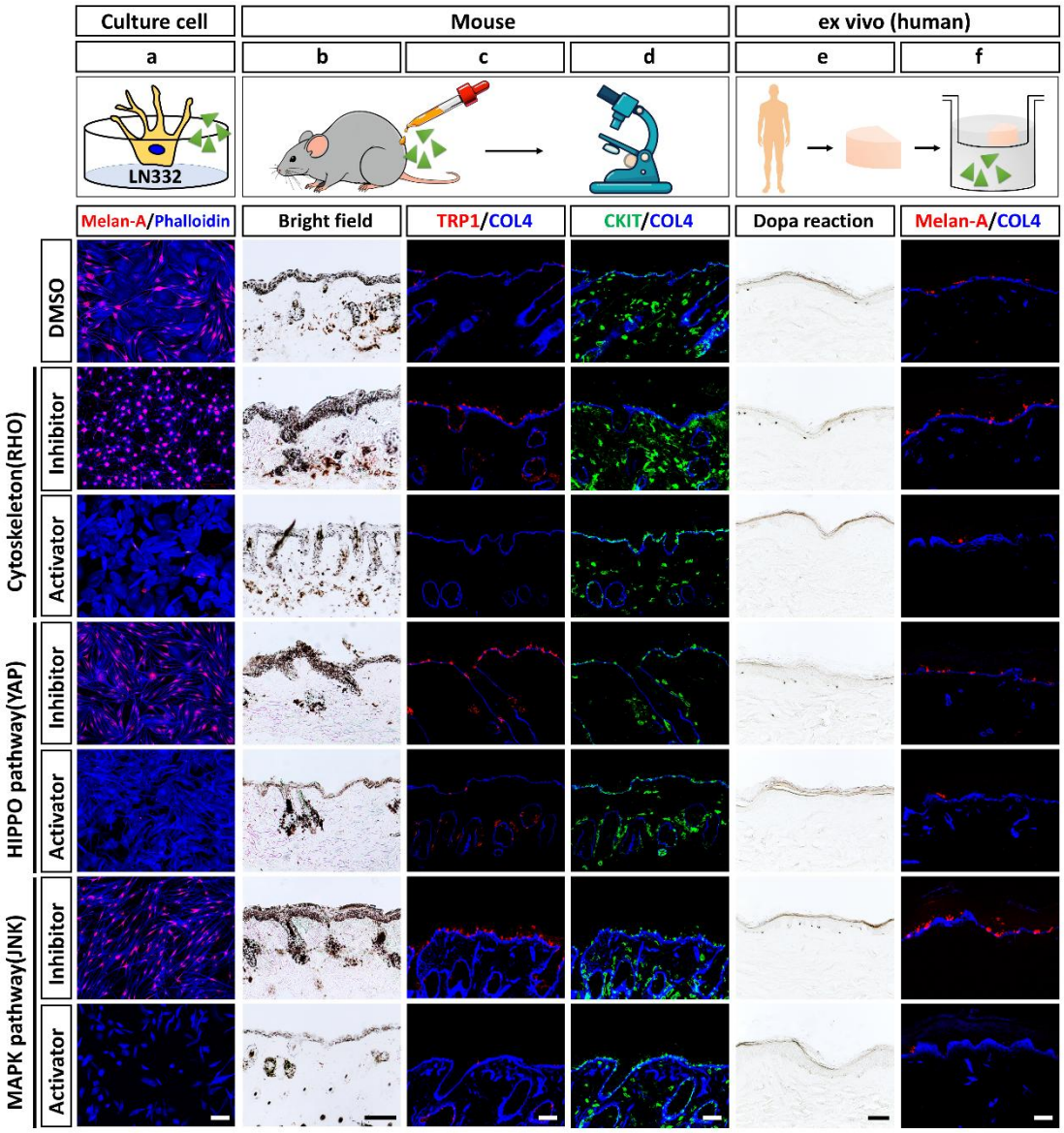

Figure 5. Evidence of Melanocyte Dedifferentiation in Vitiligo Patients. a. DOPA reaction and immunostaining analysis of perilesional vitiliginous skin (vitiligo-PL). Scale bar: 100 μm. **b.** Effects of SOX9 overexpression on melanogenic protein expression. Scale bar: 100 μm. **c.** Impact of SOX9 knockdown on melanocyte differentiation status. Scale bar: 100 μm. **d.** Spatial transcriptome analysis of perilesional vitiliginous skin.

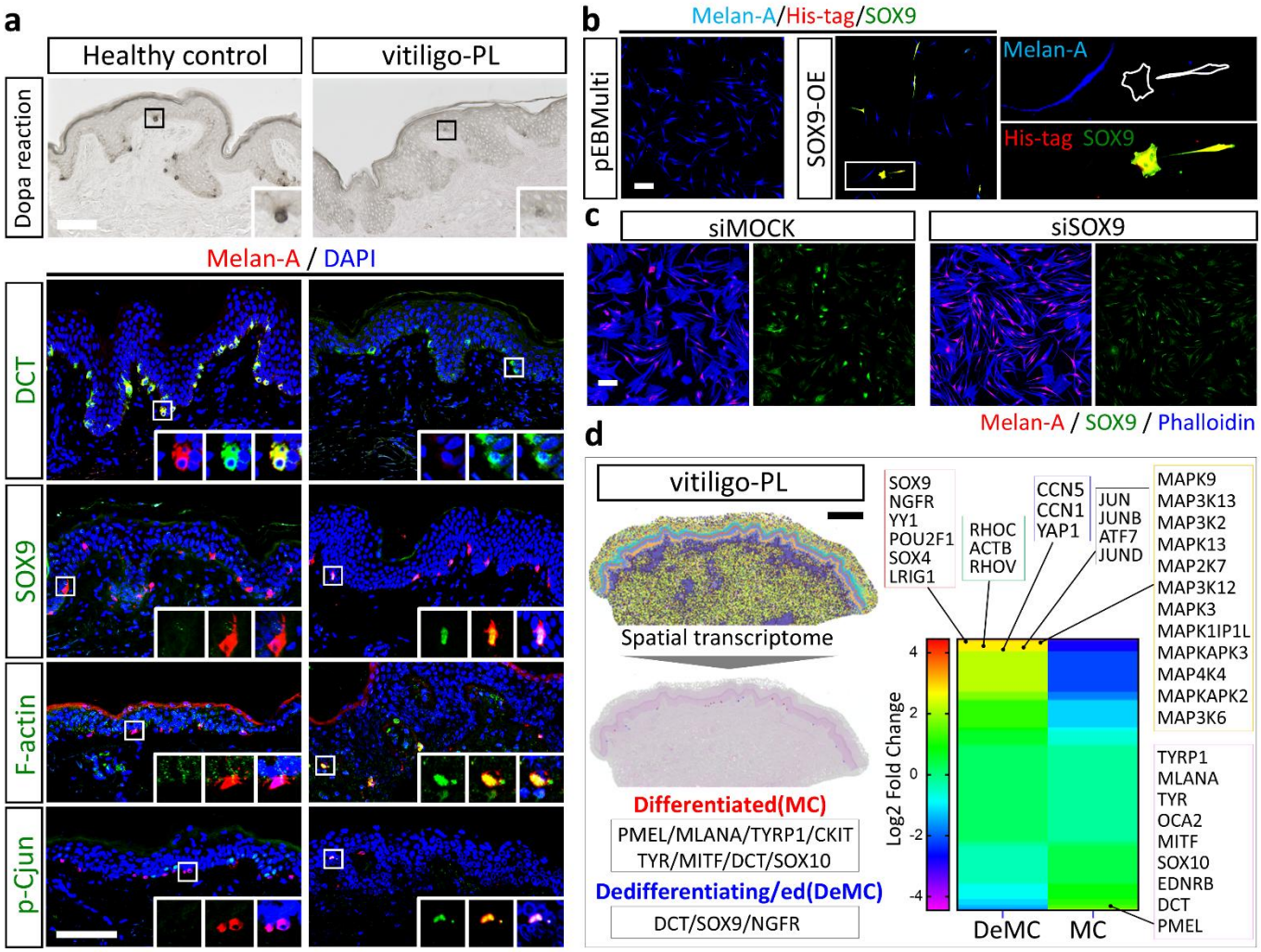

Figure 6. Therapeutic Efficacy of Dedifferentiation Inhibitors. a. Concentration-dependent effects of laminin-332 on pigmentation in 3D skin model. **b.** Pattern formation by localized laminin-332 treatment. **c.** Therapeutic effects of dedifferentiation inhibitors in 3D skin model. Scale bar: 50 μm. **d.** Therapeutic effects of dedifferentiation inhibitors in rhododendrol-induced mouse model of vitiligo. Scale bar: 100 μm. **e.** Therapeutic effects of dedifferentiation inhibitors in perilesional vitiliginous skin explants. Scale bar: 200 μm. **f.** Illustration of melanocyte state in healthy control and vitiligo skin.

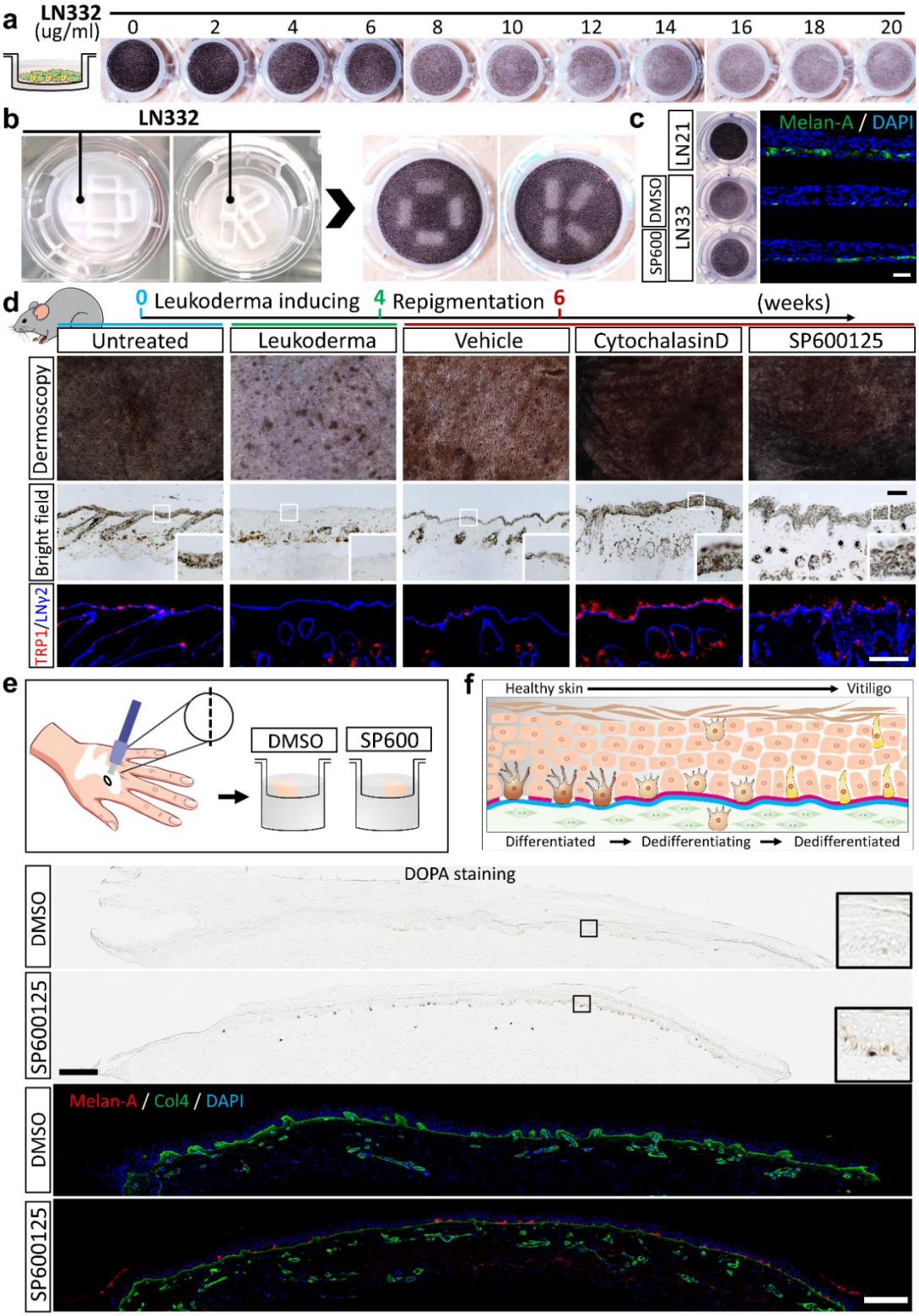

References

1. Bibeau, K.*, et al.* Mental Health and Psychosocial Quality-of-Life Burden Among Patients With Vitiligo: Findings From the Global VALIANT Study. *JAMA dermatology* **159**, 1124-1128 (2023).
2. Abdel-Malek, Z.A.*, et al.* The enigma and challenges of vitiligo pathophysiology and treatment. *Pigment cell & melanoma research* **33**, 778-787 (2020).
3. van den Boorn, J.G.*, et al.* Autoimmune destruction of skin melanocytes by perilesional T cells from vitiligo patients. *J. Invest. Dermatol.* **129**, 2220-2232 (2009).
4. Boukhedouni, N.*, et al.* Type-1 cytokines regulate MMP-9 production and E-cadherin disruption to promote melanocyte loss in vitiligo. *JCI Insight* **5**(2020).
5. Wagner, R.Y.*, et al.* Altered E-Cadherin Levels and Distribution in Melanocytes Precede Clinical Manifestations of Vitiligo. *J. Invest. Dermatol.* **135**, 1810-1819 (2015).
6. Gauthier, Y., Cario-Andre, M., Lepreux, S., Pain, C. & Taieb, A. Melanocyte detachment after skin friction in non lesional skin of patients with generalized vitiligo. *Br. J. Dermatol.* **148**, 95-101 (2003).
7. Jian, Z.*, et al.* Impaired activation of the Nrf2-ARE signaling pathway undermines H2O2-induced oxidative stress response: a possible mechanism for melanocyte degeneration in vitiligo. *J. Invest. Dermatol.* **134**, 2221-2230 (2014).
8. Bastonini, E.*, et al.* A protective role for autophagy in vitiligo. *Cell Death Dis.* **12**, 318 (2021).
9. Bellei, B.*, et al.* Vitiligo: a possible model of degenerative diseases. *PLoS One* **8**, e59782 (2013).
10. Luthold, C.*, et al.* Melanocyte differentiation and mechanosensation are differentially modulated by distinct extracellular matrix proteins. *bioRxiv*, 2024.2010.2004.616635 (2024).
11. Ranson, M., Posen, S. & Mason, R.S. Extracellular matrix modulates the function of human melanocytes but not melanoma cells. *Journal of cellular physiology* **136**, 281-288 (1988).
12. Hedley, S., Gawkrodger, D.J., Weetman, A.P. & MacNeil, S. Investigation of the influence of extracellular matrix proteins on normal human melanocyte morphology and melanogenic activity. *The British journal of dermatology* **135**, 888-897 (1996).
13. Panuncio, A.L. & Vignale, R. Ultrastructural studies in stable vitiligo. *Am. J. Dermatopathol.* **25**, 16-20 (2003).
14. Yang, F.*, et al.* Disorganisation of basement membrane zone architecture impairs melanocyte residence in vitiligo. *The Journal of Pathology* **264**, 30-41 (2024).
15. Martinez-Esparza, M., Jimenez-Cervantes, C., Solano, F., Lozano, J.A. & Garcia-Borron, J.C. Mechanisms of melanogenesis inhibition by tumor necrosis factor-alpha in B16/F10 mouse melanoma cells. *Eur. J. Biochem.* **255**, 139-146 (1998).
16. Kim, D.S., Park, S.H. & Park, K.C. Transforming growth factor-beta1 decreases melanin synthesis via delayed extracellular signal-regulated kinase activation. *Int. J. Biochem. Cell Biol.* **36**, 1482-1491 (2004).
17. Swope, V.B., Abdel-Malek, Z., Kassem, L.M. & Nordlund, J.J. Interleukins 1 alpha and 6 and tumor necrosis factor-alpha are paracrine inhibitors of human melanocyte proliferation and melanogenesis. *J. Invest. Dermatol.* **96**, 180-185 (1991).
18. Zhou, J., Ling, J., Wang, Y., Shang, J. & Ping, F. Cross-talk between interferon-gamma and interleukin-18 in melanogenesis. *J. Photochem. Photobiol. B* **163**, 133-143 (2016).
19. Wang, Y.*, et al.* Roles of MMP-2 and MMP-9 and their associated molecules in the pathogenesis of keloids: a comprehensive review. *Front. Pharmacol.* **15**, 1444653 (2024).
20. Burgeson, R.E. & Christiano, A.M. The dermal-epidermal junction. *Current opinion in cell biology* **9**, 651-658 (1997).
21. Yamada, M. & Sekiguchi, K. Chapter Six - Molecular Basis of Laminin–Integrin Interactions. in *Current Topics in Membranes*, Vol. 76 (ed. Miner, J.H.) 197-229 (Academic Press, 2015).
22. Haass, N.K., Smalley, K.S.M., Li, L. & Herlyn, M. Adhesion, migration and communication in melanocytes and melanoma. *Pigment cell research* **18**, 150-159 (2005).
23. Fukunaga-Kalabis, M.*, et al.* CCN3 controls 3D spatial localization of melanocytes in the human skin through DDR1. *The Journal of cell biology* **175**, 563-569 (2006).
24. Loftus, S.K.*, et al.* Comparison of melanoblast expression patterns identifies distinct classes of genes. *Pigment cell & melanoma research* **22**, 611-622 (2009).
25. Mort, R.L., Jackson, I.J. & Patton, E.E. The melanocyte lineage in development and disease. *Development* **142**, 620-632

(2015).
26. Comandante-Lou, N., Baumann, D.G. & Fallahi-Sichani, M. AP-1 transcription factor network explains diverse patterns of cellular plasticity in melanoma cells. *Cell reports* **40**, 111147 (2022).
27. Koo, J.H. & Plouffe, S.W. Induction of AP-1 by YAP/TAZ contributes to cell proliferation and organ growth. **34**, 72-86 (2020).
28. Whitmarsh, A.J. & Davis, R.J. Transcription factor AP-1 regulation by mitogen-activated protein kinase signal transduction pathways. *Journal of molecular medicine (Berlin, Germany)* **74**, 589-607 (1996).
29. Dunn, K.J.*, et al.* WNT1 and WNT3a promote expansion of melanocytes through distinct modes of action. *Pigment cell research* **18**, 167-180 (2005).
30. Zabierowski, S.E.*, et al.* Direct reprogramming of melanocytes to neural crest stem-like cells by one defined factor. *Stem cells (Dayton, Ohio)* **29**, 1752-1762 (2011).
31. Zhong, Z., Jiao, Z. & Yu, F.-X. The Hippo signaling pathway in development and regeneration. *Cell reports* **43**(2024).
32. Renshaw, M.W., Toksoz, D. & Schwartz, M.A. Involvement of the small GTPase rho in integrin-mediated activation of mitogen-activated protein kinase. *The Journal of biological chemistry* **271**, 21691-21694 (1996).
33. Du, M., Liu, M., Fan, F., Shi, P. & Tu, M. Structure, Function, and Nutrition of Lactoferrin. in *Mineral Containing Proteins : Roles in Nutrition* (ed. Zhao, G.) 33-61 (Springer Singapore, Singapore, 2017).
34. Custurone, P. & Di Bartolomeo, L. Role of Cytokines in Vitiligo: Pathogenesis and Possible Targets for Old and New Treatments. **22**(2021).
35. Zhang, C.
36. Inoue, S. & Katayama, I. Rhododendrol-induced leukoderma update II: Pathophysiology, mechanisms, risk evaluation, and possible mechanism-based treatments in comparison with vitiligo. **48**, 969-978 (2021).
37. Xu, P.*, et al.* Effects of EGFR-TKI on epidermal melanin unit integrity: Therapeutic implications for hypopigmented skin disorders. *Pigment cell & melanoma research* **37**, 514-529 (2024).
38. Cook, A.L., Smith, A.G., Smit, D.J., Leonard, J.H. & Sturm, R.A. Co-expression of SOX9 and SOX10 during melanocytic differentiation in vitro. *Experimental cell research* **308**, 222-235 (2005).
39. Shakhova, O.*, et al.* Antagonistic cross-regulation between Sox9 and Sox10 controls an anti-tumorigenic program in melanoma. *PLoS genetics* **11**, e1004877 (2015).
40. Harris, M.L., Baxter, L.L., Loftus, S.K. & Pavan, W.J. Sox proteins in melanocyte development and melanoma. *Pigment cell & melanoma research* **23**, 496-513 (2010).
41. Stüfchen, I.*, et al.* Sox9 regulates melanocytic fate decision of adult hair follicle stem cells. *iScience* **26**, 106919 (2023).
42. Hedstrand, H.*, et al.* The Transcription Factors SOX9 and SOX10 Are Vitiligo Autoantigens in Autoimmune Polyendocrine Syndrome Type I *. *Journal of Biological Chemistry* **276**, 35390-35395 (2001).
43. Zhu, S.*, et al.* GnRHa/Stanozolol Combined Therapy Maintains Normal Bone Growth in Central Precocious Puberty. *Frontiers in endocrinology* **12**, 678797 (2021).
44. Sbardella, D.*, et al.* α-dystroglycan is a potential target of matrix metalloproteinase MMP-2. *Matrix Biology* **41**, 2-7 (2015).
45. Pellegrini, C.*, et al.* Melanocytes--a novel tool to study mitochondrial dysfunction in Duchenne muscular dystrophy. *J. Cell. Physiol.* **228**, 1323-1331 (2013).
46. Martin, P.T. The dystroglycanopathies: the new disorders of O-linked glycosylation. *Seminars in pediatric neurology* **12**, 152-158 (2005).
47. Yaar, M. & Park, H.-Y. Melanocytes: A Window into the Nervous System. *Journal of Investigative Dermatology* **132**, 835-845 (2012).
48. Fillmore, H.L., VanMeter, T.E. & Broaddus, W.C. Membrane-type matrix metalloproteinases (MT-MMPs): expression and function during glioma invasion. *J. Neurooncol.* **53**, 187-202 (2001).
49. Kumar, R., Parsad, D., Kanwar, A. & Kaul, D. Development of melanocye-keratinocyte co-culture model for controls and vitiligo to assess regulators of pigmentation and melanocytes. *Indian journal of dermatology, venereology and leprology* **78**, 599-604 (2012).
50. Kawakami, T. Surgical procedures and innovative approaches for vitiligo regenerative treatment and melanocytorrhagy. *The Journal of dermatology* **49**, 391-401 (2022).
51. Kumar, R., Parsad, D., Kanwar, A.J. & Kaul, D. Altered levels of Ets-1 transcription factor and matrix metalloproteinases in melanocytes from patients with vitiligo. *The British journal of dermatology* **165**, 285-291 (2011).
52. Tobin, D.J., Swanson, N.N., Pittelkow, M.R., Peters, E.M. & Schallreuter, K.U. Melanocytes are not absent in lesional skin

of long duration vitiligo. *The Journal of pathology* **191**, 407-416 (2000).

53. Robinson, R.L.*, et al.* Comparative STAT3-Regulated Gene Expression Profile in Renal Cell Carcinoma Subtypes. *Frontiers in Oncology* **9**(2019).
54. Takahashi, K. & Yamanaka, S. Induction of pluripotent stem cells from mouse embryonic and adult fibroblast cultures by defined factors. *Cell* **126**, 663-676 (2006).
55. Pesaresi, M., Sebastian-Perez, R. & Cosma, M.P. Dedifferentiation, transdifferentiation and cell fusion: in vivo reprogramming strategies for regenerative medicine. *The FEBS Journal* **286**, 1074-1093 (2019).
56. Merrell, A.J. & Stanger, B.Z. Adult cell plasticity in vivo: de-differentiation and transdifferentiation are back in style. *Nature Reviews Molecular Cell Biology* **17**, 413-425 (2016).
57. Shibata, S.*, et al.* Selective Laminin-Directed Differentiation of Human Induced Pluripotent Stem Cells into Distinct Ocular Lineages. *Cell reports* **25**, 1668-1679.e1665 (2018).
58. Üstün, Y.*, et al.* Dual role of laminin-511 in regulating melanocyte migration and differentiation. *Matrix Biology* **80**, 59-71 (2019).
59. Yui, S.*, et al.* YAP/TAZ-Dependent Reprogramming of Colonic Epithelium Links ECM Remodeling to Tissue Regeneration. *Cell stem cell* **22**, 35-49.e37 (2018).
60. Manderfield, L.J.*, et al.* Pax3 and hippo signaling coordinate melanocyte gene expression in neural crest. *Cell reports* **9**, 1885-1895 (2014).
61. Yardman-Frank, J.M. & Fisher, D.E. Skin pigmentation and its control: From ultraviolet radiation to stem cells. *Experimental dermatology* **30**, 560-571 (2021).
62. Lan, C.C.E.*, et al.* FK506 promotes melanocyte and melanoblast growth and creates a favourable milieu for cell migration via keratinocytes: possible mechanisms of how tacrolimus ointment induces repigmentation in patients with vitiligo. *British Journal of Dermatology* **153**, 498-505 (2005).
63. Tang, D.*, et al.* SRplot: A free online platform for data visualization and graphing. *PLoS One* **18**, e0294236 (2023).
64. Yang, F.*, et al.* Uncoupling of ER/Mitochondrial Oxidative Stress in mTORC1 Hyperactivation-Associated Skin Hypopigmentation. *J. Invest. Dermatol.* **138**, 669-678 (2018).

Supplementary Information

Extended Data Figures

Extended Data Figure 1. Immunofluorescent staining of various laminin chains, including antibody against laminins (LNs), laminin alpha 1-5 (LNα1, LNα2, LNα3, LNα4, LNα5), laminin beta 1-3 (LNβ1, LNβ2, LNβ3) and laminin gamma 1-3 ((LNγ1, LNγ2, LNγ3) at the dermal-epidermal junction in normal human skin sections. Melanocytes, identified using a melanocyte-specific marker, are indicated by white arrowheads. Each panel shows a different laminin chain. Scale bar: 5 μm.

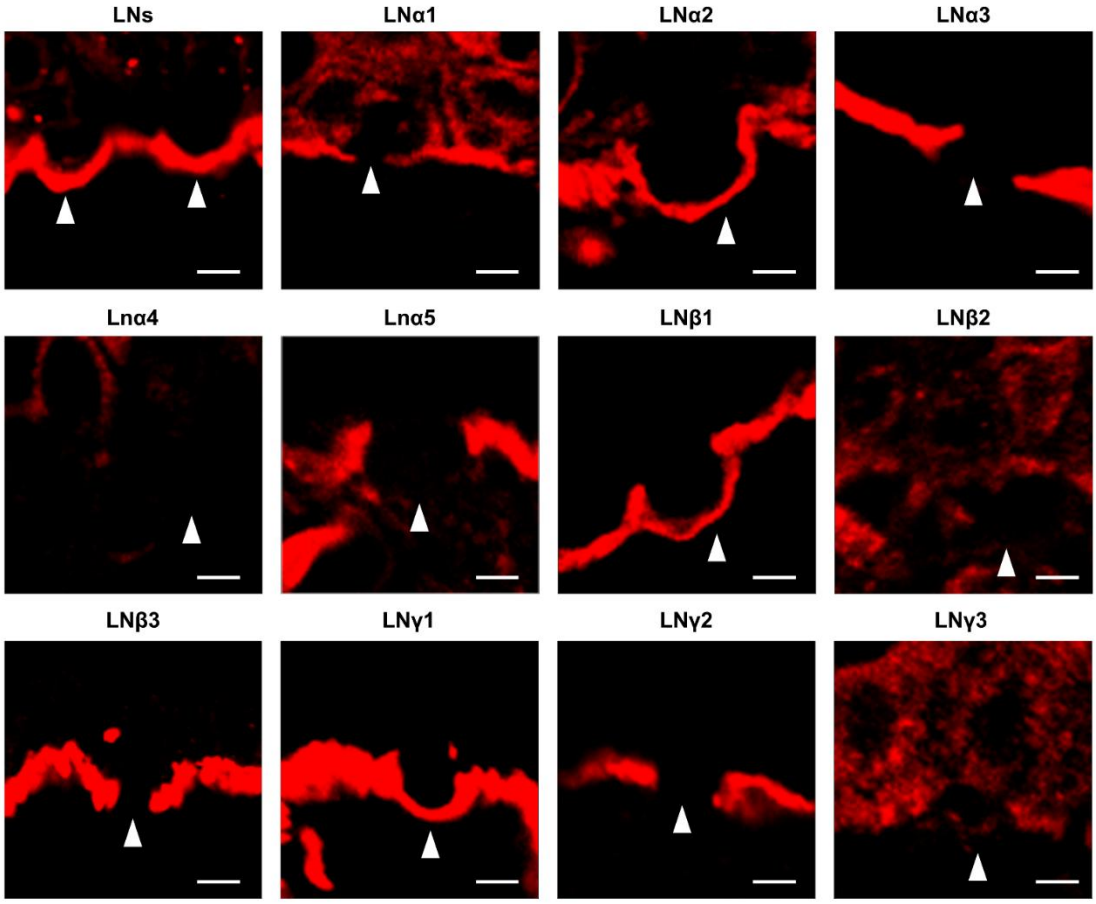

Extended Data Figure 2. Analysis of exceptional cases showing continuous laminin-332 distribution without direct basement membrane contact in skin from healthy control. Upper panel shows immuno-electron microscopy of laminin α3, lower right shows immunofluorescence staining. Arrows indicate melanocytes in contact with basement membrane, arrowheads indicate melanocytes without basement membrane contact. Scale bar: 10 µm.

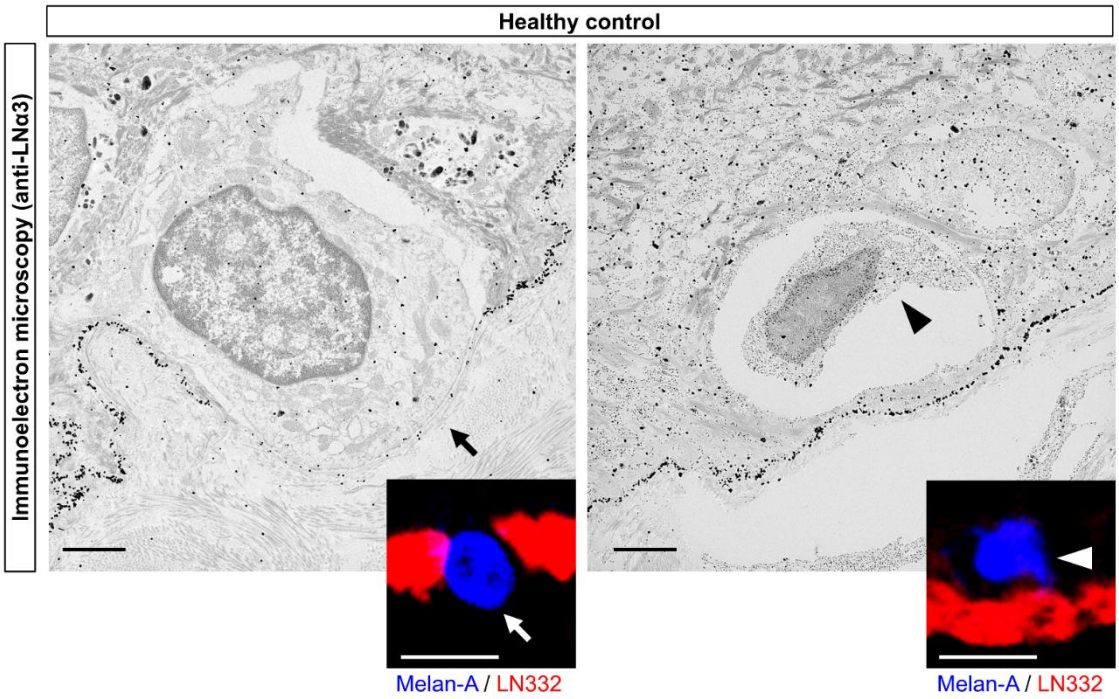

Extended Data Figure 3. Analysis of integrin expression patterns in normal human melanocytes in skin tissue from three healthy controls. Scale bar: 50 μm.

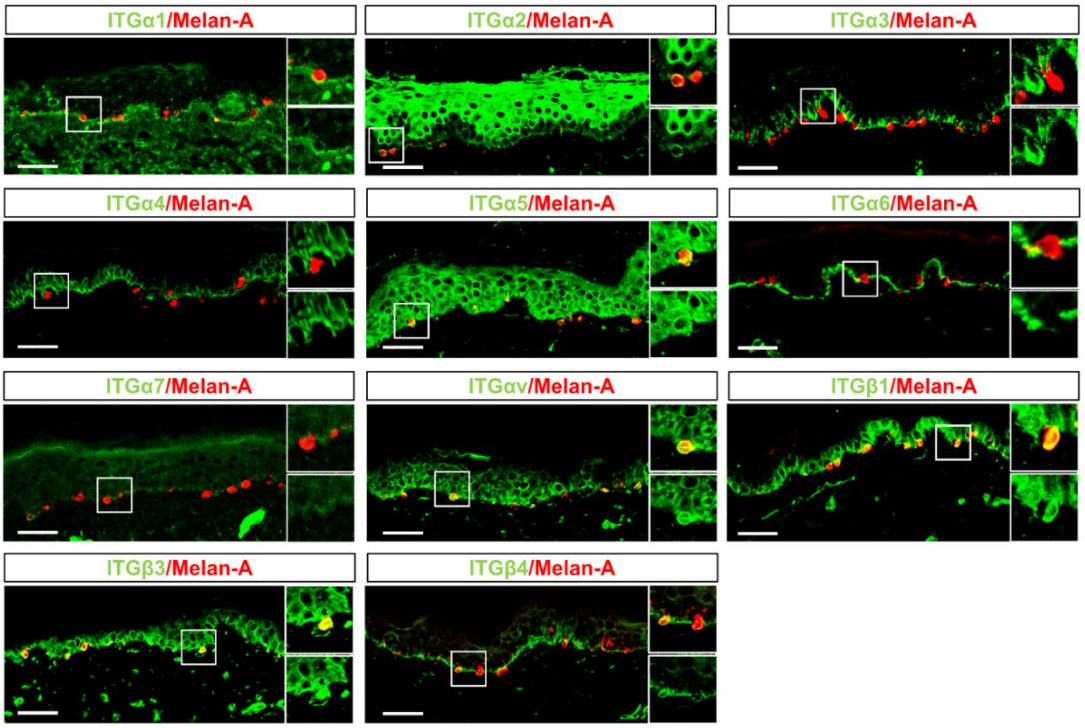

Extended Data Figure 4. Detailed analysis of integrin-laminin α2 protein interactions in keratinocytes and melanocytes in skin tissue from three healthy controls. Scale bar: 50 μm.

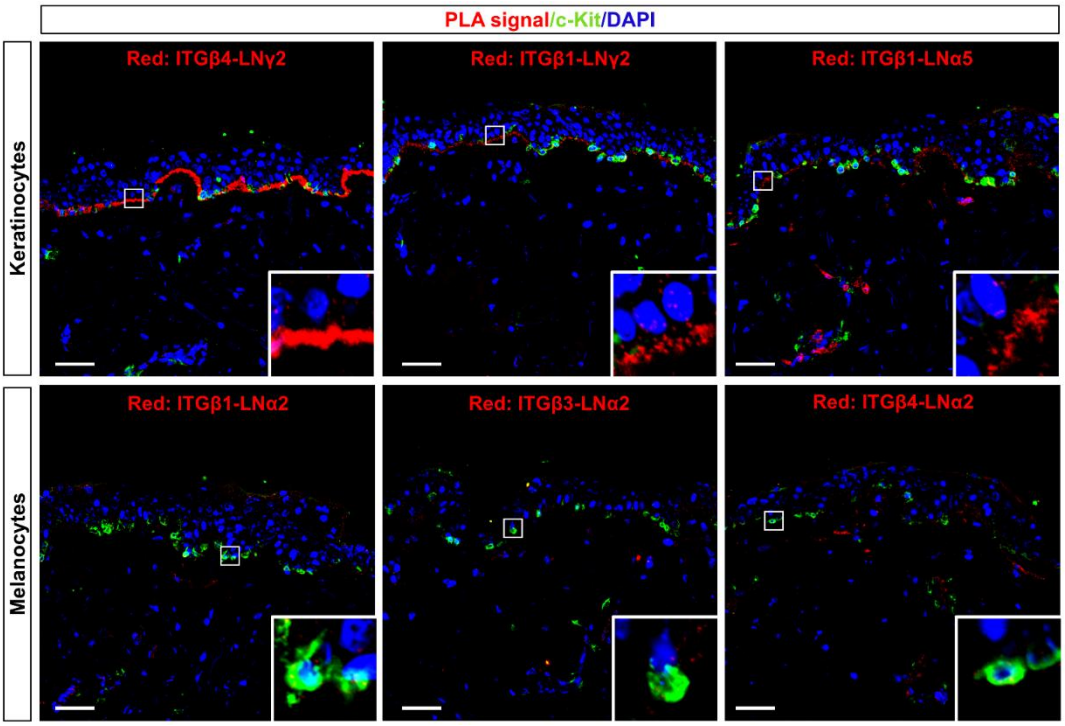

Extended Data Figure 5. Analysis of cell morphology and melanogenic protein expression across multiple melanocyte lines following laminin-332 treatment. Scale bar: 100 μm.

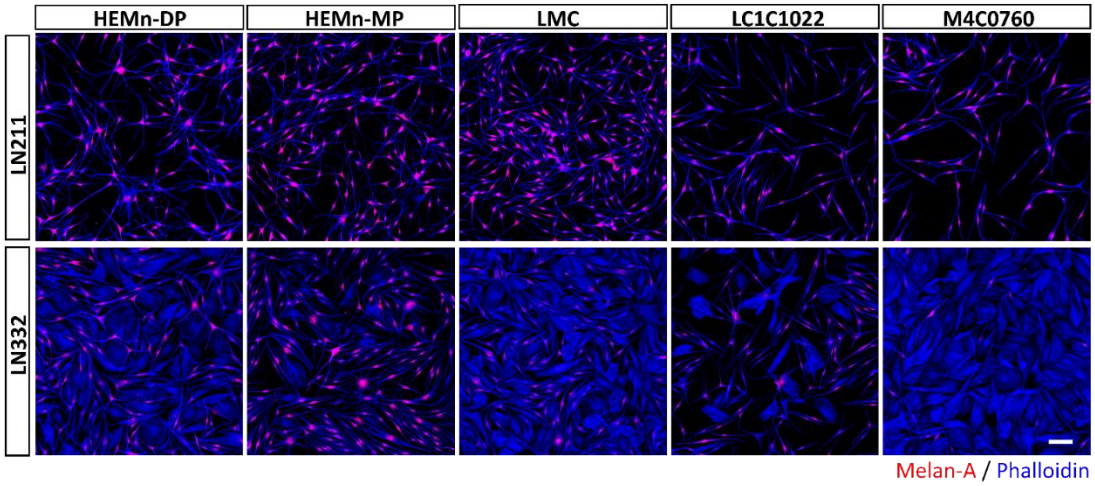

Extended Data Figure 6. Comparative analysis of precursor cell marker expression between melanoblasts and laminin-332-induced dedifferentiated cells. Scale bar: 100 μm.

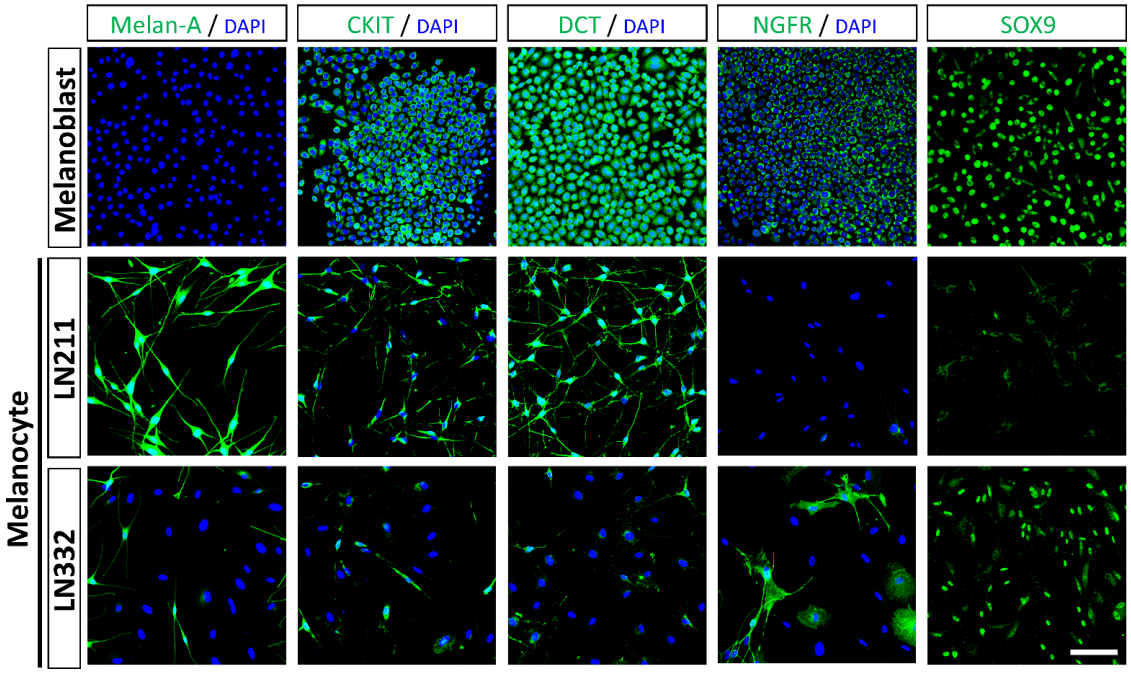

Extended Data Figure 7. Multi-parameter immunostaining analysis of laminin-332-treated melanocytes showing distinct cell populations. **a-d** show cells after laminin-332 treatment. Arrowheads in **c** indicate NGFR/Melan-A double-negative dedifferentiated cells. Arrowheads in **d** indicate SOX9/Melan-A double-negative dedifferentiated cells. Scale bar: 100 μm.

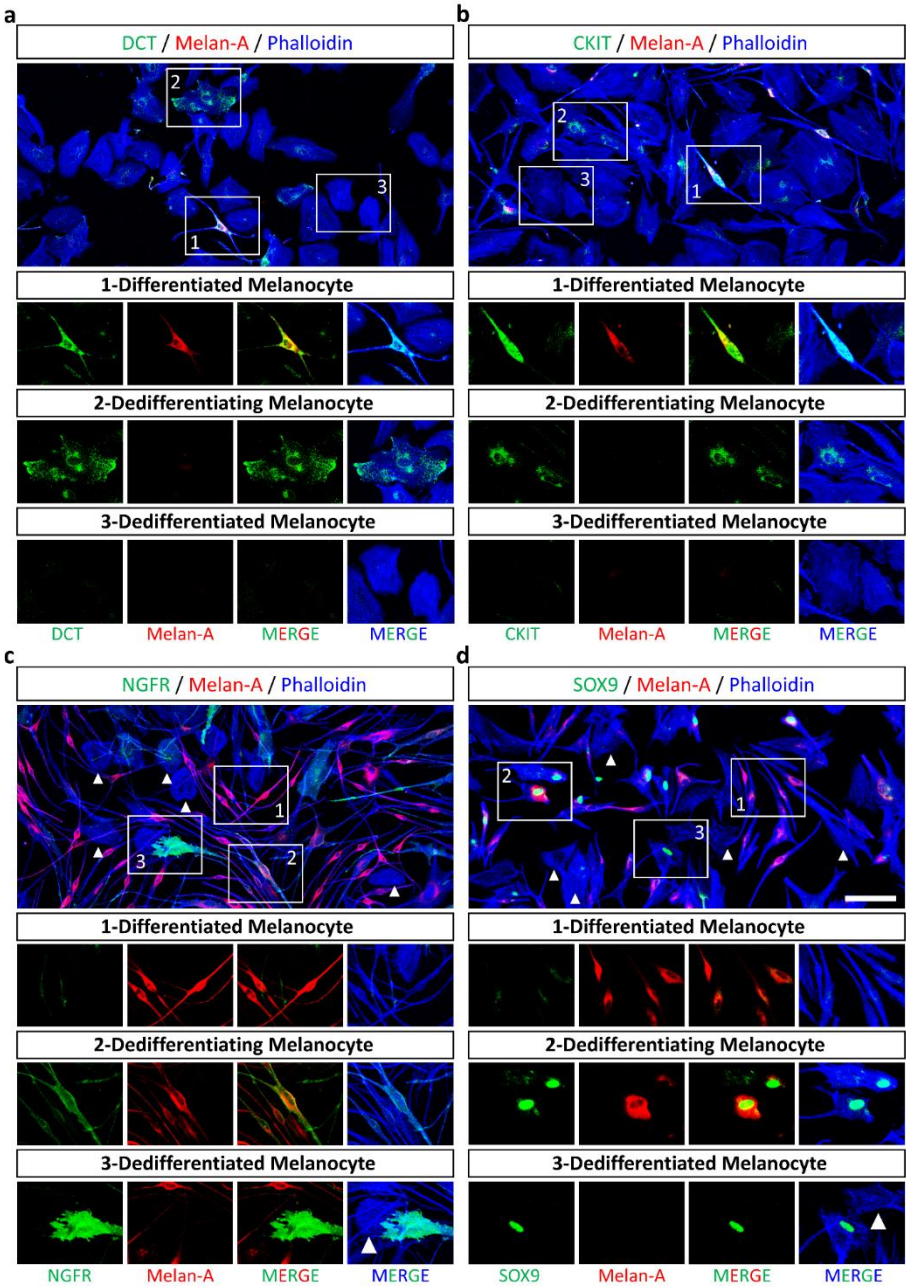

Extended Data Figure 8. Analysis of integrin subtype effects on laminin-332-induced melanocyte dedifferentiation. **a**. Immunofluorescence analysis of integrin expression in cultured melanocytes. Scale bar: 100 μm. **b**. Analysis of dedifferentiation rates following integrin knockdown. Blue phalloidin single-positive cells indicate dedifferentiated cells. Scale bar: 100 μm.

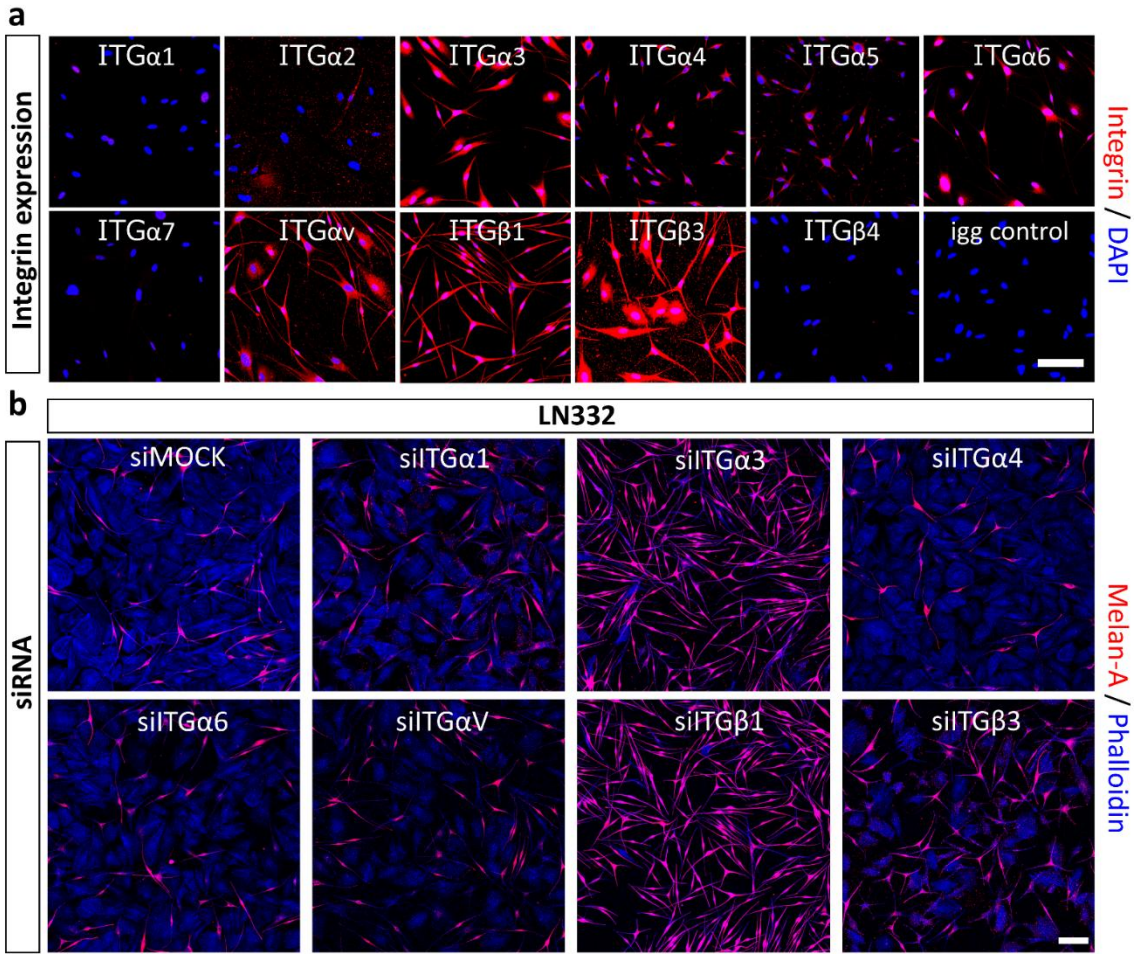

Extended Data Figure 9. Western blot analysis of cytoskeleton components, Hippo pathway, MAPK pathway, and AP-1 family members in laminin-332-induced dedifferentiated cells. Lane 1: control cells treated with laminin-211. Lane 2: cells after laminin-332 treatment. Lower panel shows quantification. Note that CCN1 and CCN2 were undetectable in control cells, resulting in relative expression values of 4,912% and 4,189%, respectively; these values were truncated in the graph due to scale limitations.

* P<0.05, ** P<0.01, *** P<0.001, NS: not significant.

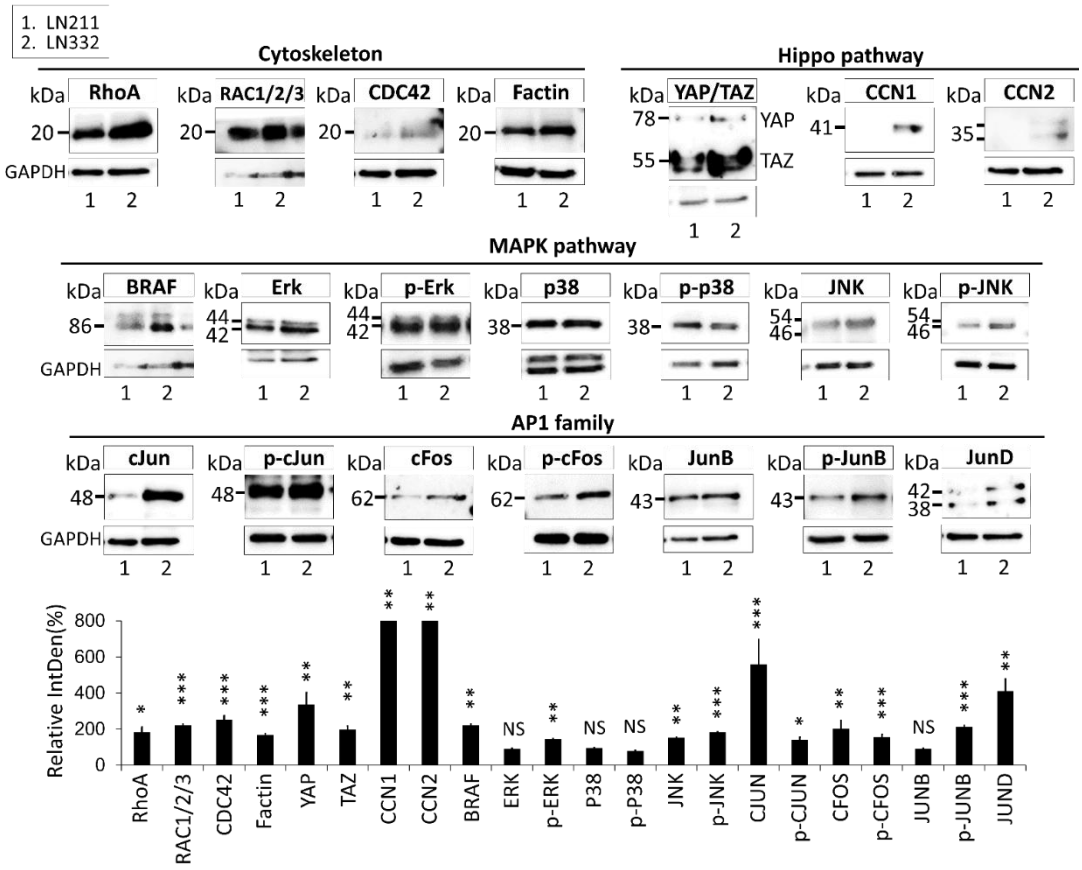

Extended Data Figure 10. Analysis of vitiligo-associated factors' effects on melanocyte dedifferentiation. **a.** Analysis of melanocyte dedifferentiation induced by WNT5A, inflammatory factors, ROS, and rhododendrol. Scale Bar: 100 μm. **b.** Effects of different JAK inhibitors on laminin-332-induced dedifferentiation. Scale Bar: 100 μm.

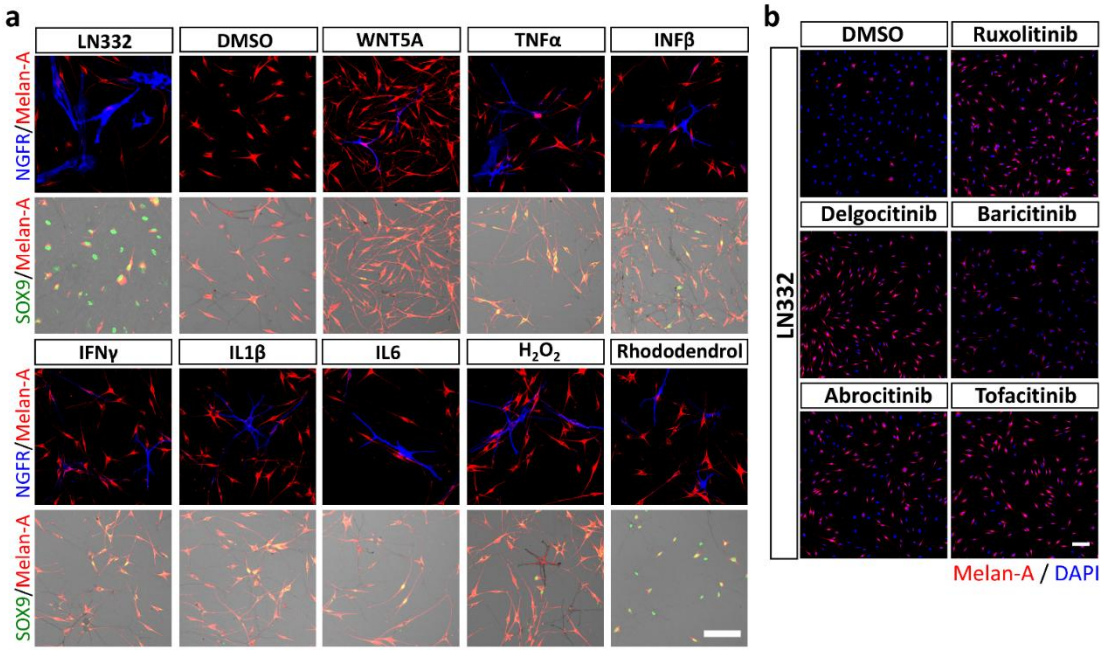

Extended Data Figure 11. Analysis of various tyrosine kinase inhibitors' effects on melanocyte dedifferentiation. Scale Bar: 100 μm.

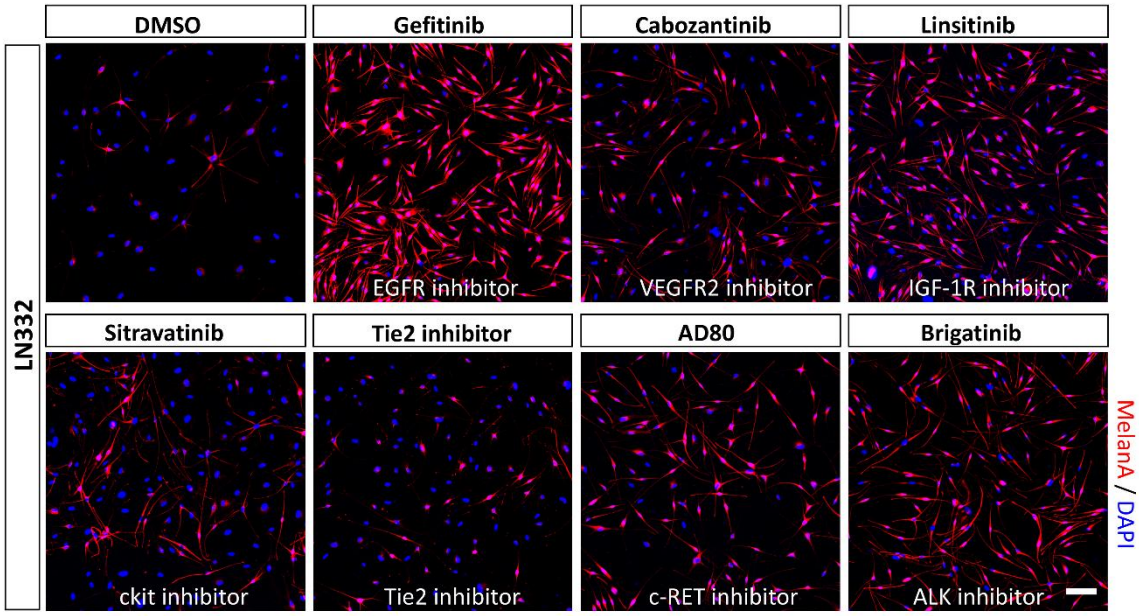

Extended Data Figure 12. Schematic summary of signaling pathways involved in melanocyte dedifferentiation.

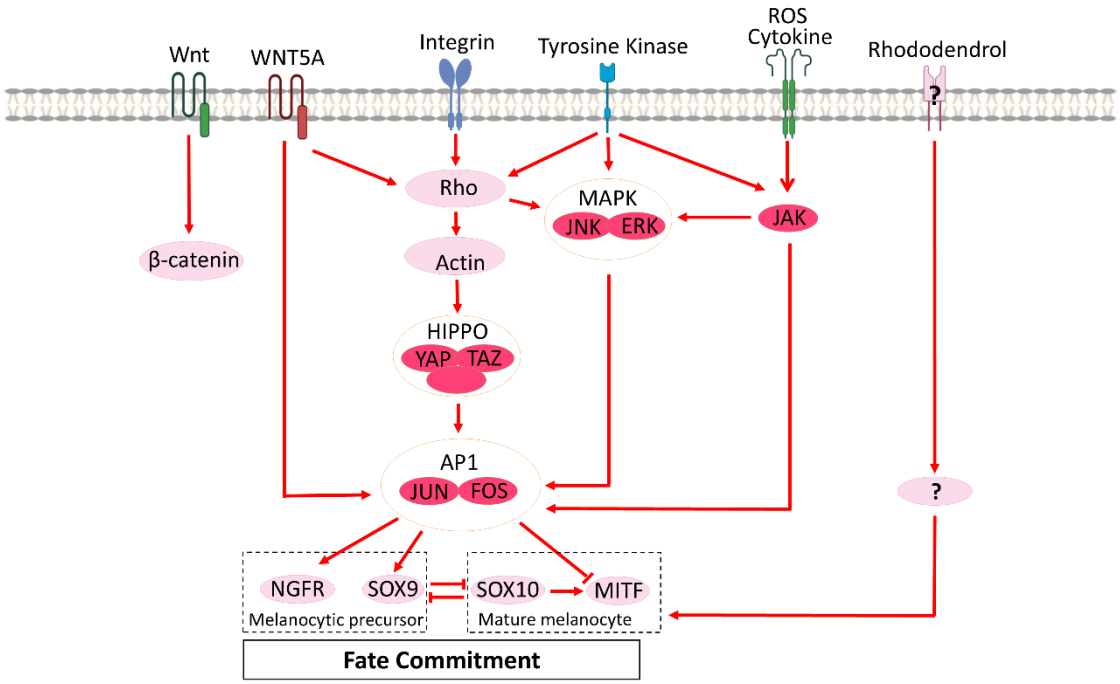

Extended Data Figure 13. Identify dedifferentiating and dedifferentiated melanocytes in vitiligo. **a.** Analysis of c-Kit and NGFR expressions in vitiligo perilesional melanocytes. Scale Bar: 50 μm. **b-c.** Analysis of dedifferentiated melanocyte location in lesional (vitiligo-L) and perilesional (vitiligo-PL) vitiliginous skin. Arrowheads indicate cells detaching from basal layer, arrows indicate cells entering dermis. Scale bar: 50 μm.

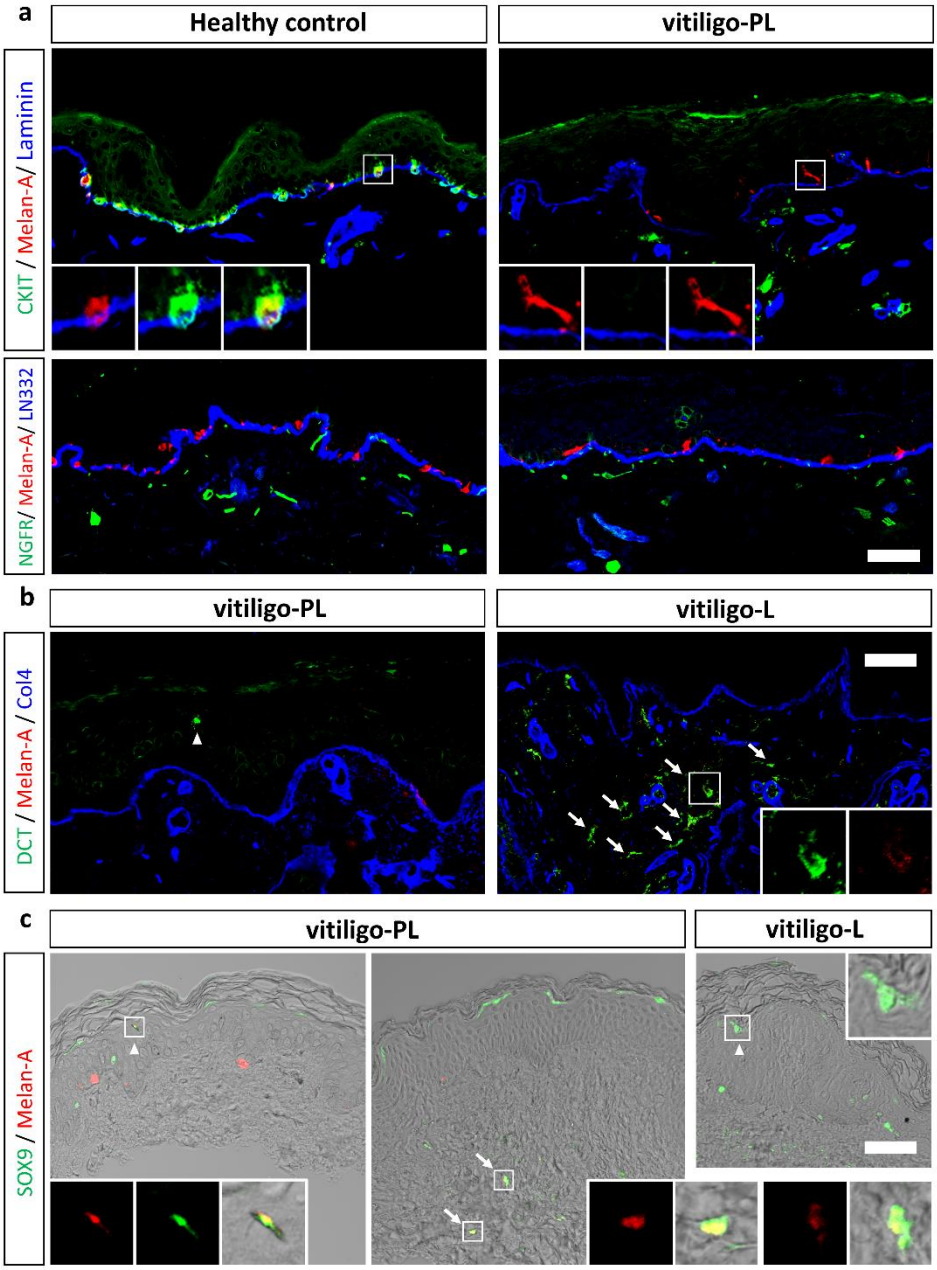

Extended Data Figure 14. Analysis of melanoblasts retention in epidermis. **a.** Schematic of 3D skin model. **b.** Gross appearance of 3D skin model. **c.** Analysis of melanocyte and melanoblast distribution in 3D skin model. Scale bar: 50 μm.

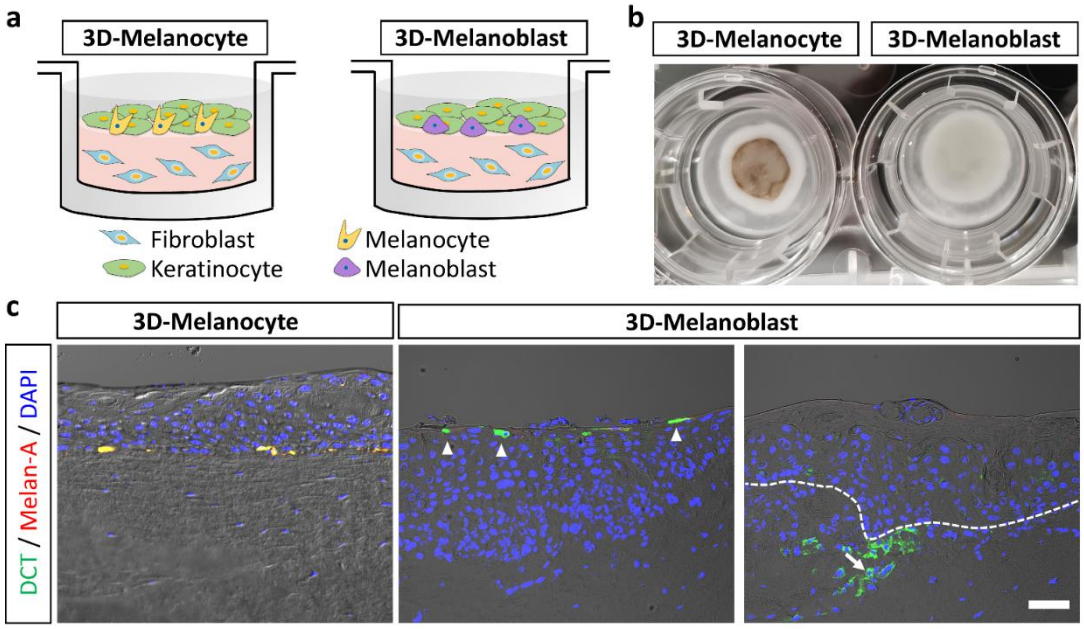

Extended Data Figure 15. Dynamics of dedifferentiating melanocytes in rhododendrol-induced leukoderma in mice. **a.** Analysis of depigmentation phenotype in K14-Kitl mice induced by rhododendrol. **b.** Dose-dependent effects of rhododendrol on melanocyte dedifferentiation. Scale bar: 50 μm. Arrowheads indicate c-Kit/DCT-positive but TRP1-negative undifferentiating melanocytes.

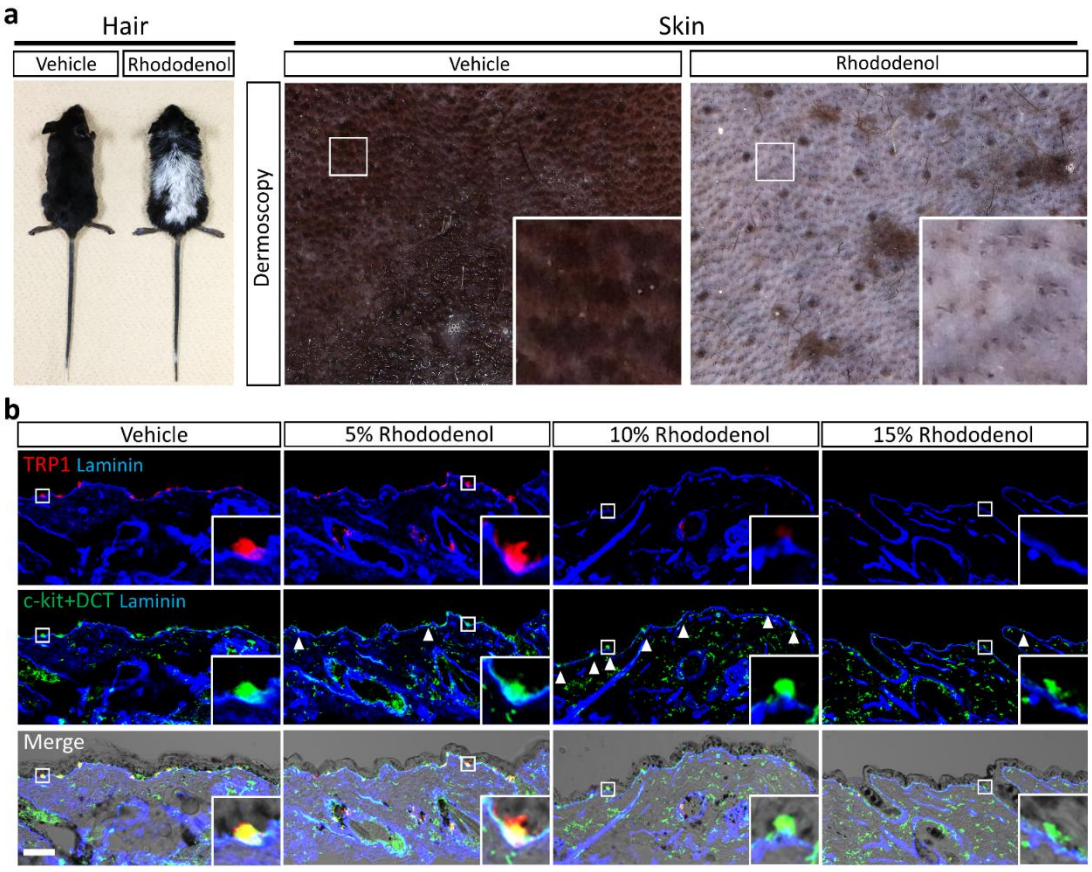

Extended Data Figure 16. Dynamics of dedifferentiating melanocytes in vitiligo patient skin. **a.** Schematic of ex vivo culture system for vitiligo patient skin. **b.** Analysis of melanocyte differentiation status following SP600125 treatment. Scale bar: 50 μm.

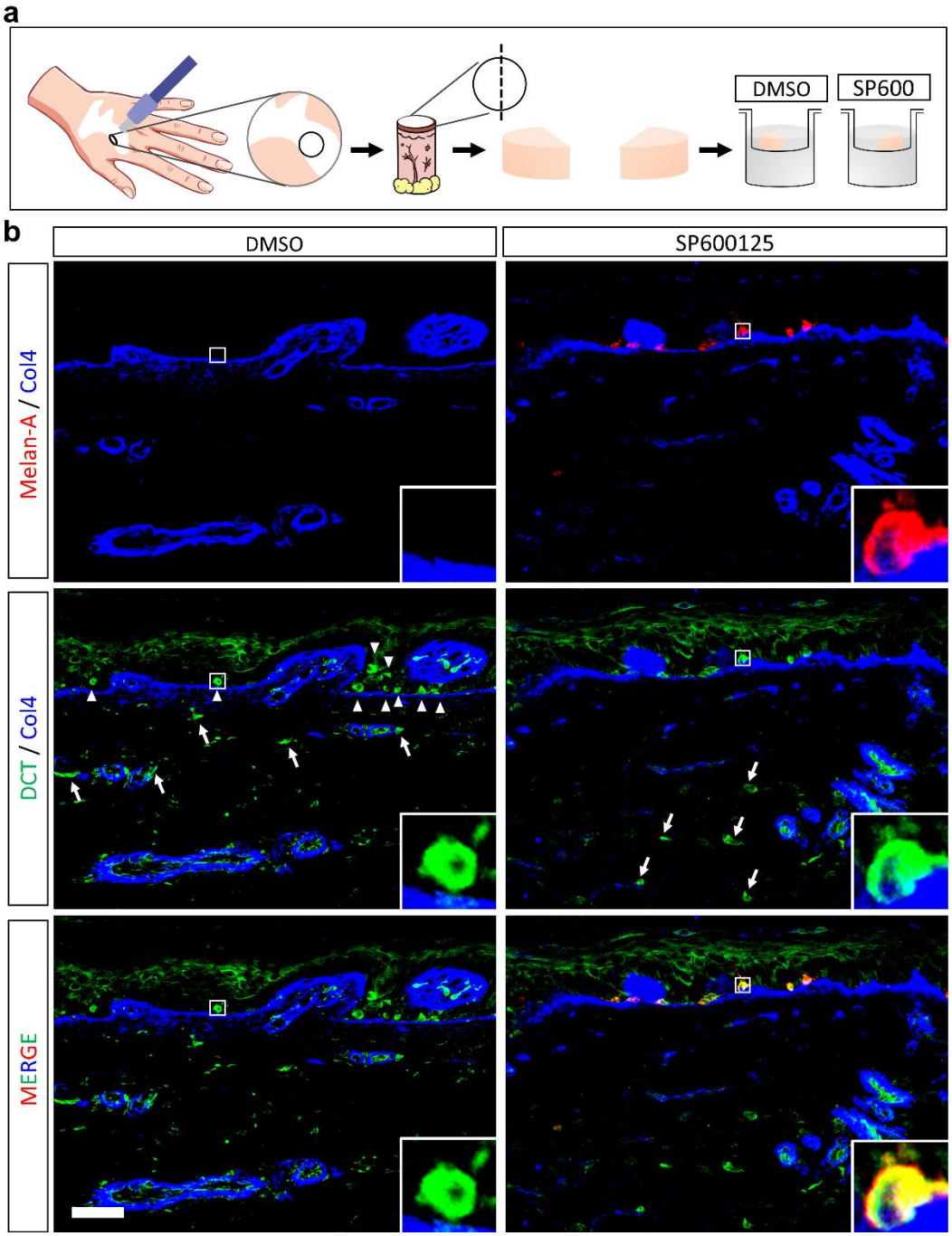

Extended Data Figure 17. Dedifferentiating melanocytes in 3D skin model. **a.** Schematic of culture 3D skin model. **b.** Analysis of mature and dedifferentiating melanocyte populations in laminin-332-treated 3D skin model. Scale bar: 50 μm.

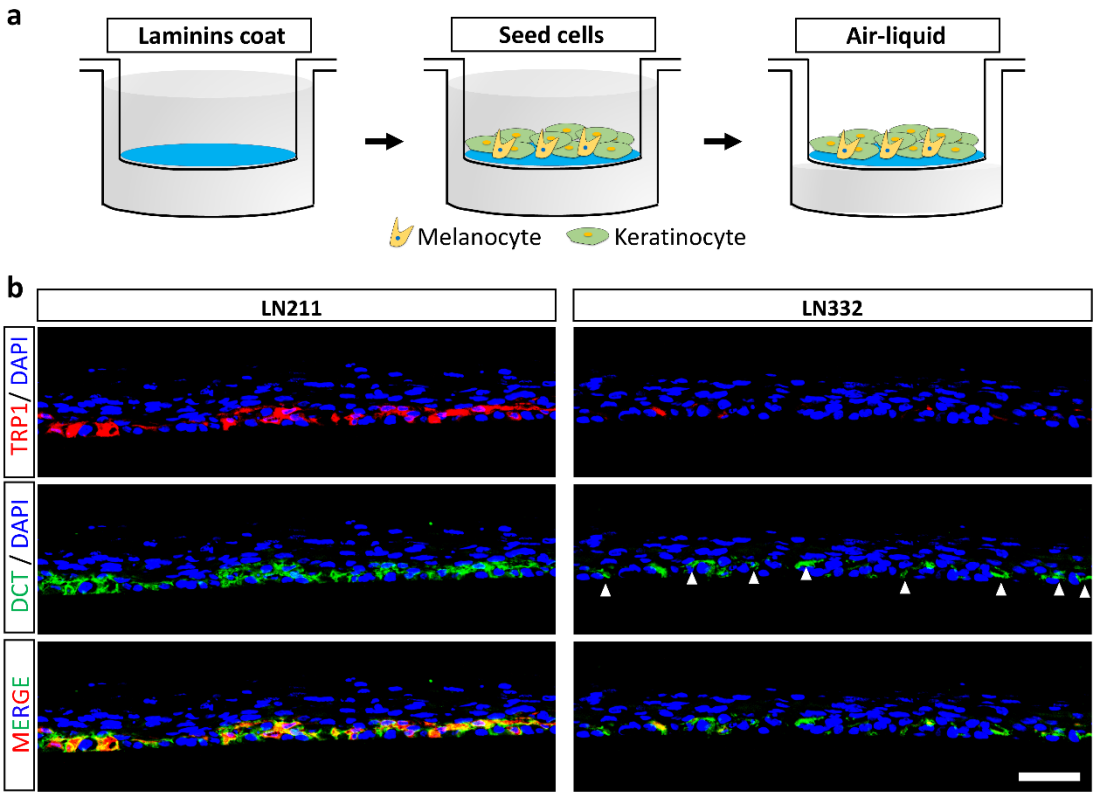

Extended Data Figure 18. Analysis of MT-MMP-mediated laminin-332 degradation. **a.** Analysis of MT-MMP expression in normal epidermal melanocytes. Scale bar: 50 μm. **b.** Comparison of MT-MMP expression across cell lines. **c.** MT-MMP expression in melanocytes and melanoblasts. Scale bar: 100 μm. **d.** Analysis of MT-MMP-mediated laminin-332 degradation capacity. Scale bar: 100 μm.

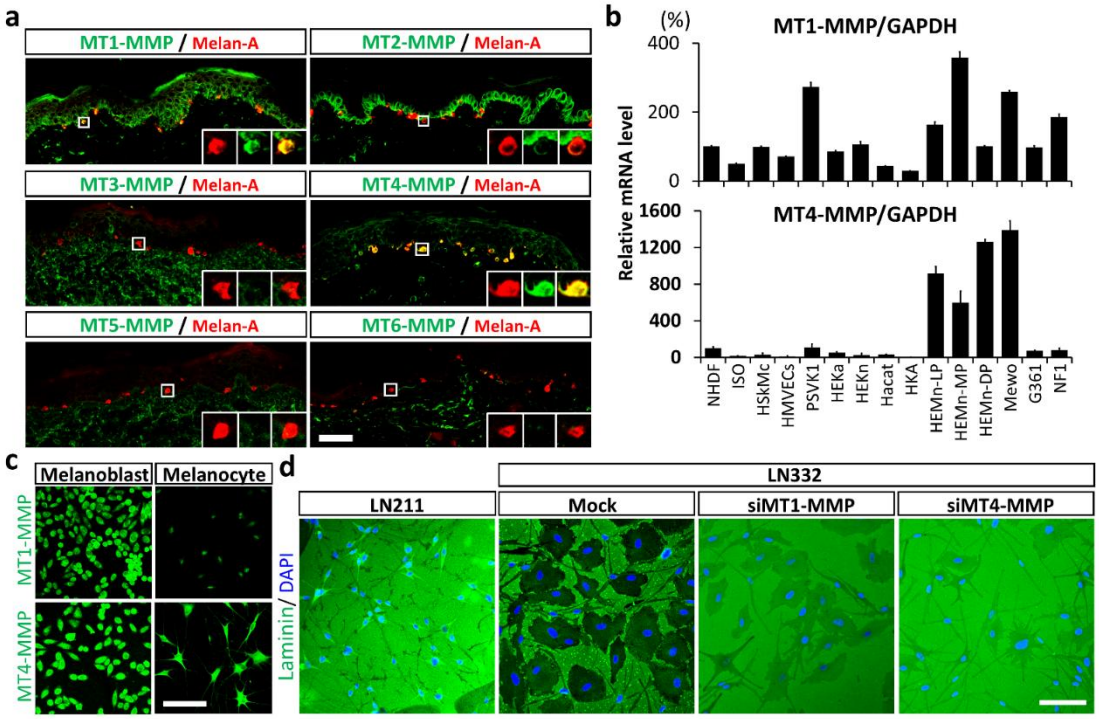

Extended Data Figure 19. Analysis of MT-MMP expression in vitiligo patients. **a.** Analysis of MT4-MMP expression in vitiligo perilesional melanocytes. Scale bar: 50 µm. **b.** Analysis of MT1-MMP expression in vitiligo perilesional melanocytes. Scale bar: 50 µm. **c.** Analysis of MT-MMP expression in mouse melanocytes. Scale bar: 50 µm.

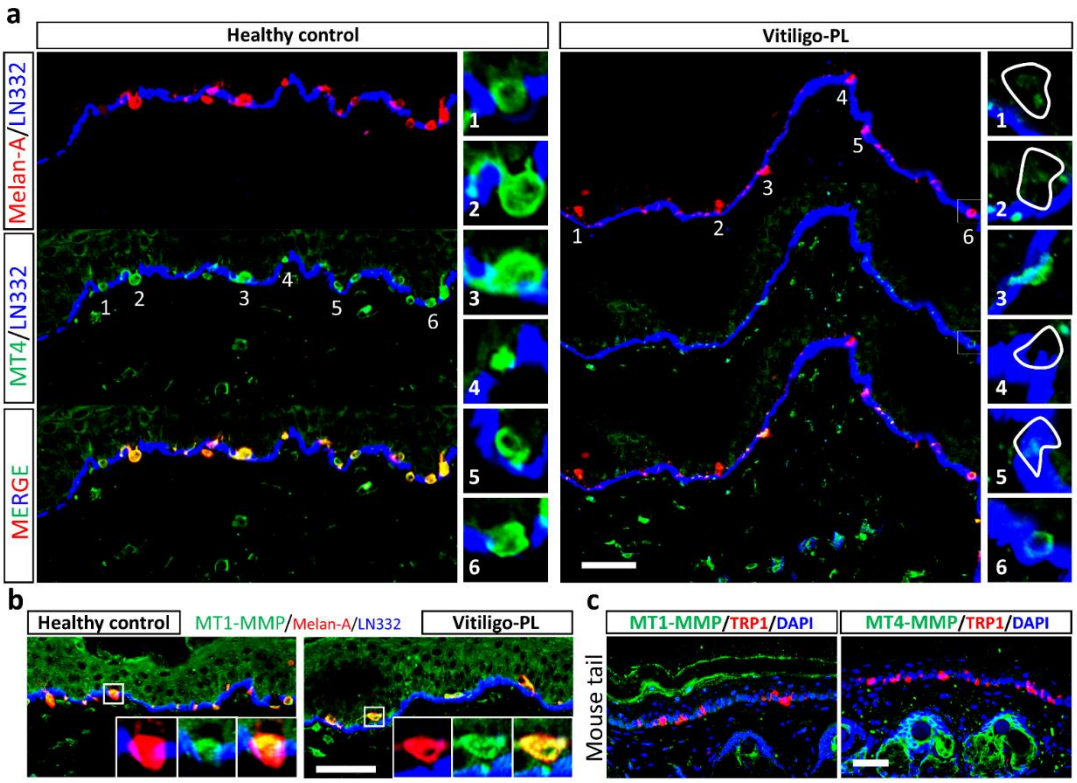

Extended Data Figure 20. Analysis of dystroglycan expression in vitligo skin and cultured melanocytes. **a.** Analysis of dystroglycan expression in healthey skin and vitiligo perilesional melanocytes. Scale bar: 50 μm. **b.** Analysis of dystroglycan expression in cultured melanocytes after laminin-332 treatment. Scale bar: 100 μm.

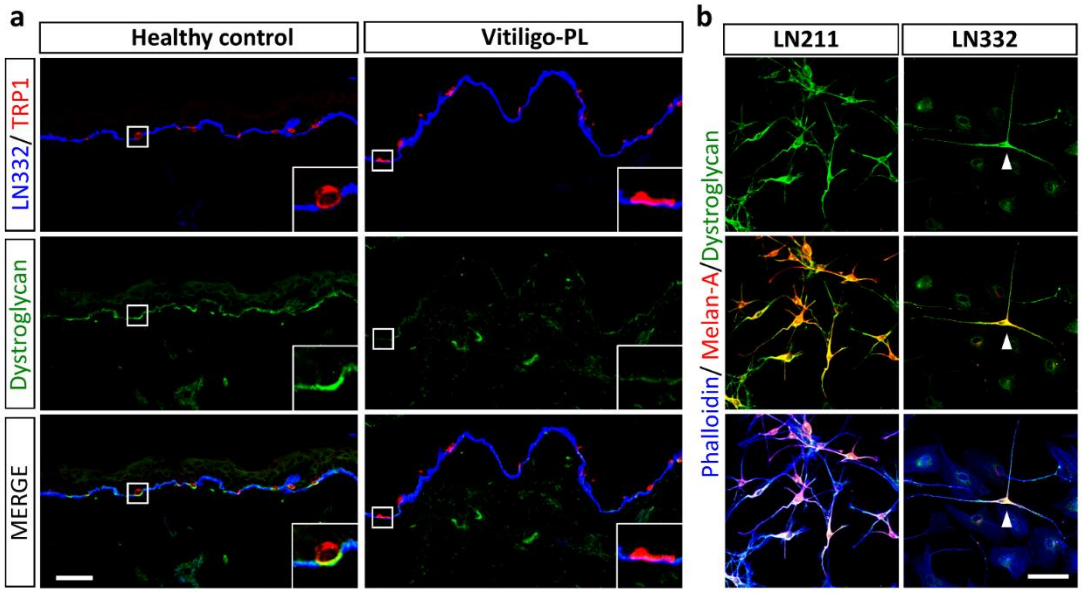

Extended Data Figure 21. Analysis of dystroglycan function in epidermal melanocyte retention. **a.** Analysis of dystroglycan expression in melanocytes and melanoblasts. Scale bar: 100 μm. **b.** Analysis of dystroglycan expression and laminin-332 distribution in perifollicular melanocyte subtypes. Scale bar: 100 μm.

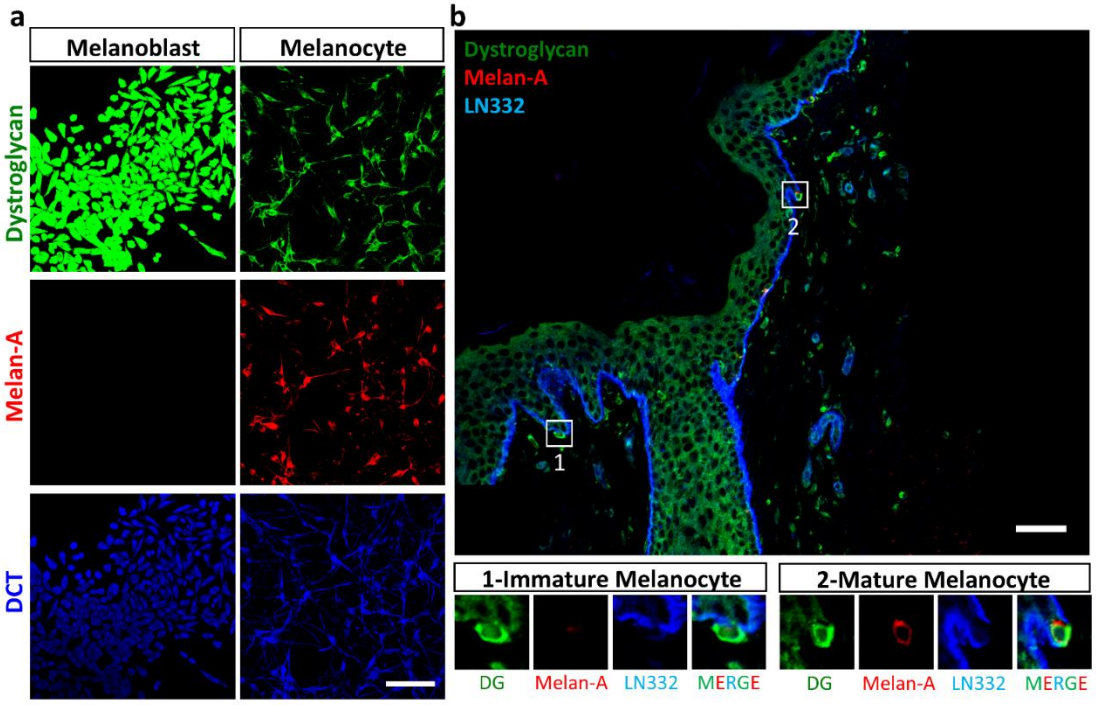

Extended Data Figure 22. Analysis of laminin-211 expression in skin from C57BL6/J mice. **a.** Analysis of laminin α2 expression in tail skin and dorsal skin from C57BL6/J mice. Scale bar: 100 μm. **b.** Analysis of laminin α2 expression in inner and outside of ear skin from C57BL6/J mice. Scale bar: 100 μm.

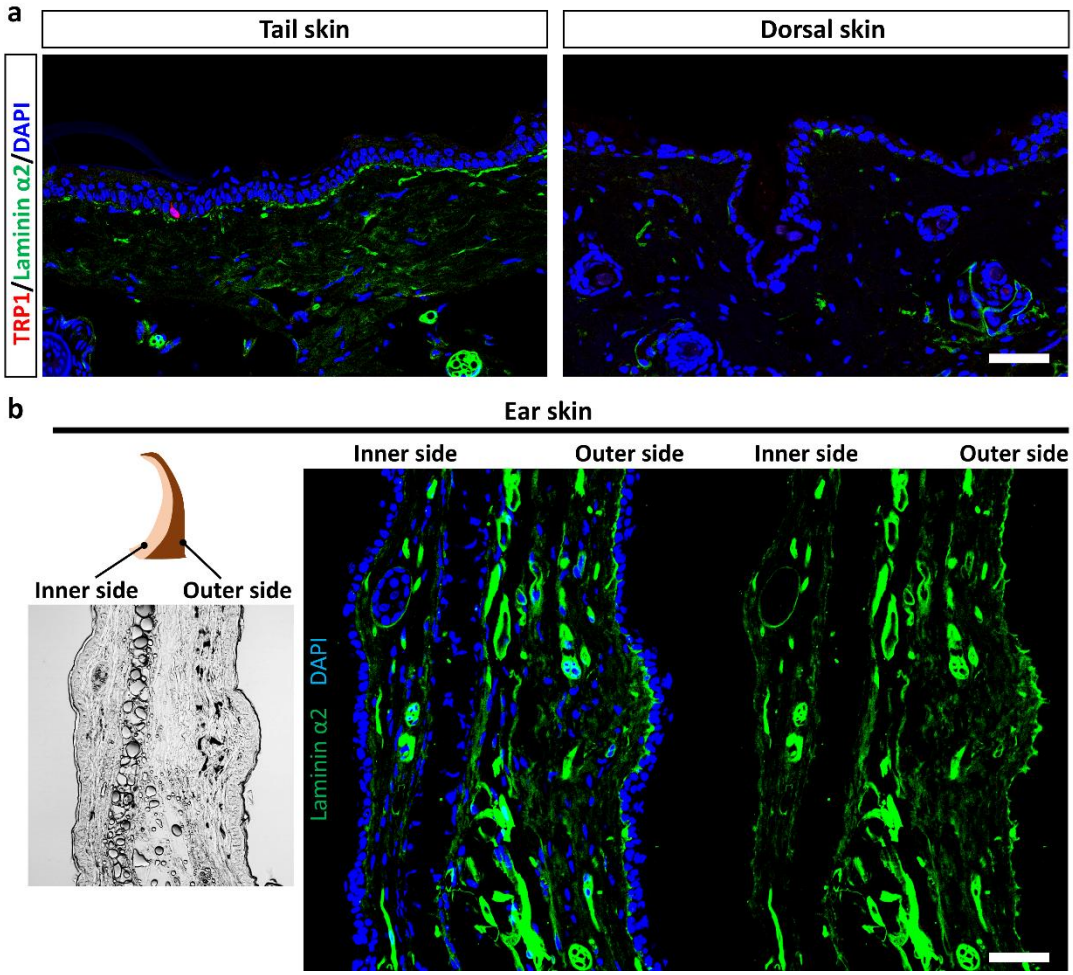

Supplementary table

Table S1. Clinical characteristics of the patients

Patient No.	Sex	Age (years)	Type	Biopsy site	Activity
1[§]	M	72	Nonsegmental vitiligo	Back	Progressive
2[§]	F	49	Nonsegmental vitiligo	Lumbar	Stable
3	M	44	Nonsegmental vitiligo	Back	Progressive
4	F	33	Nonsegmental vitiligo	Axilla	Progressive
5	F	71	Nonsegmental vitiligo	Elbow	Stable
6[§]	F	23	Nonsegmental vitiligo	Abdomen	Stable
7[§]	M	30	Nonsegmental vitiligo	Lateral abdomen	Progressive
8[§]	F	20	Nonsegmental vitiligo	Abdomen	Progressive
9	M	68	Nonsegmental vitiligo	Back	Progressive
10	F	49	Nonsegmental vitiligo	Abdomen	Progressive
11	F	62	Nonsegmental vitiligo	Neck	Stable
12	M	47	Nonsegmental vitiligo	Axilla	Progressive
13[*]	M	76	Nonsegmental vitiligo	Wrist	Progressive
14[*]	F	69	Nonsegmental vitiligo	Back of the hand	Progressive
15	M	47	Nonsegmental vitiligo	Arm	Stable

[§]Samples for electron microscopy.

*Samples for *ex vivo* skin culture.

Abbreviations: F: female; M: male.

Table S2. List of primary antibodies used for immunofluorescence and immunohistochemical analyses.

Antibody Name	Host, Isotype and Subclass	Dilution	Catalog No.	Company Name
Laminin	Rabbit	1:100	ab11575	Abcam
Laminin α1	Mouse IgG1	1:100	AMAb91091	Sigma-Aldrich
Laminin α2	Rat IgG1	1:100	L0663	Sigma-Aldrich
Laminin α3	Mouse IgG2a	1:100	FDV-0024	Funakoshi
Laminin α4	Rabbit	1:100	SAB4501719	Sigma-Aldrich
Laminin α5	Mouse IgG1	1:100	MABT39	Sigma-Aldrich
Laminin β1	Rat IgG1	1:100	ab44941	Abcam
Laminin β2	Mouse IgG1	1:100	AMAb91096	Sigma-Aldrich
Laminin β3	Rabbit	1:100	26795-1-AP	Proteintech
Laminin γ1	Rat IgG2a	1:100	ab80580	Abcam
Laminin γ2	Rabbit	1:100	SAB2700481	Sigma-Aldrich
Laminin 332	Mouse IgG1	1:100	ab78286	Abcam
Integrin α1	Mouse IgG1	1:100	NBP2-76478	Novus Biologicals
Integrin α2	Mouse IgG1	1:100	NBP2-76483	Novus Biologicals
Integrin α3	Mouse IgG2a	1:100	NBP1-97691	Novus Biologicals
Integrin α4	Rabbit	1:100	19676-1-AP	Proteintech
Integrin α5	Rabbit	1:100	27224-1-AP	Proteintech
Integrin α6	Mouse IgG2b	1:100	ab20142	Abcam
Integrin α7	Mouse IgG1	1:100	ab195959	Abcam
Integrin αv	Rabbit	1:100	100563-T08	Sino Biological
Integrin β1	Mouse IgG2a	1:100	ab30388	Abcam
Integrin β1	Rabbit	1:100	PA532887	Thermo Fisher
Integrin β3	Rabbit	1:100	100458-T08	Sino Biological
Integrin β4	Rabbit	1:100	PB9007	Boster Bio
Dystroglycan	Rabbit	1:100	11017-1-AP	Proteintech
DDR	Goat	1:100	AF2396	R&D Systems
Melan-A	Mouse IgG2b	1:100	917901	BioLegend

c-kit	Goat	1:100	AF332	R&D Systems
c-kit	Rat IgG2b	1:100	NBP1-43359	Novus Biologicals
PMEL	Rabbit	1:100	ab137078	Abcam
TRP1	Mouse IgG2a	1:100	917801	BioLegend
Neurofilament	Rabbit	1:100	2837	Cell Signaling Technology
COL2	Rabbit	1:100	28459-1-AP	BioLegend
α-SMA	Mouse IgG2a	1:100	M0851	Dako
SOX9	Rabbit	1:100	AB5535	Sigma-Aldrich
NGFR	Rabbit	1:100	ab52987	Abcam
DCT	Mouse IgG2a	1:100	sc-74439	Santa Cruz Biotechnology
Collagen IV	Rabbit	1:100	ab19808	Abcam
F-actin	Mouse IgM	1:100	ab205	Abcam
p-JUN	Rabbit	1:100	3270S	Cell Signaling Technology
His-Tag	Rabbit	1:100	12698	Cell Signaling Technology
MT1-MMP	Rabbit	1:100	ARG57921	Arigo biolaboratories
MT2-MMP	Rabbit	1:100	HPA040390	Sigma-Aldrich
MT3-MMP	Rabbit	1:100	HPA023693	Sigma-Aldrich
MT4-MMP	Rabbit	1:100	PA5-28219	Thermo Fisher
MT5-MMP	Rabbit	1:100	AB924	R&D Systems
MT6-MMP	Mouse IgG1	1:100	MAB11421	R&D Systems
Rabbit IgG Control	Rabbit	1:100	ab172730	Abcam
Mouse IgG Control	Mouse	1:100	ab37355	Abcam
Alexa Fluor 633 Phalloidin		1:500	A22284	Thermo Fisher

Table S3. List of secondary antibodies used for immunofluorescence and immunohistochemical analyses.

Antibody Name	Host	Dilution	Catalog No.	Company Name
Alexa Fluor® Plus 488 Goat Anti-Rabbit IgG (H+L)	Goat	1:1,000	A32731	Invitrogen
Alexa Fluor® Plus 555 Goat Anti-Rabbit IgG (H+L)	Goat	1:1,000	A32732	Invitrogen
Alexa Fluor® Plus 647 Goat Anti-rabbit IgG (H+L)	Goat	1:1,000	A32733	Invitrogen
Alexa Fluor® Plus 488 Goat Anti-mouse IgG (H+L)	Goat	1:1,000	A32723	Invitrogen
Alexa Fluor® Plus 555 Goat Anti-mouse IgG (H+L)	Goat	1:1,000	A32727	Invitrogen
Alexa Fluor® Plus 647 Goat Anti-mouse IgG (H+L)	Goat	1:1,000	A21236	Invitrogen
Goat anti-Mouse IgG1, Alexa Fluor® 488	Goat	1:1,000	A21121	Invitrogen
Goat anti-Mouse IgG1, Alexa Fluor® 555	Goat	1:1,000	A21127	Invitrogen
Goat anti-Mouse IgG1, Alexa Fluor® 647	Goat	1:1,000	A21240	Invitrogen
Goat anti-Mouse IgG2a, Alexa Fluor® 488	Goat	1:1,000	A21131	Invitrogen
Goat anti-Mouse IgG2a, Alexa Fluor® 555	Goat	1:1,000	A21137	Invitrogen
Goat anti-Mouse IgG2a, Alexa Fluor® 647	Goat	1:1,000	A21136	Invitrogen
Goat anti-Mouse IgG2b, Alexa Fluor® 488	Goat	1:1,000	A21141	Invitrogen
Goat anti-Mouse IgG2b, Alexa Fluor® 555	Goat	1:1,000	A21147	Invitrogen
Goat anti-Mouse IgG2b, Alexa Fluor® 647	Goat	1:1,000	A21242	Invitrogen
Goat anti-Rat IgG (H+L), Alexa Fluor 488	Goat	1:1,000	A11006	Invitrogen
Goat anti-Rat IgG (H+L), Alexa Fluor 555	Goat	1:1,000	A48263	Invitrogen
Goat anti-Rat IgG (H+L), Alexa Fluor 647	Goat	1:1,000	A21247	Invitrogen
Donkey anti-Goat IgG (H+L), Alexa Fluor Plus 488	Donkey	1:1,000	A32814	Invitrogen
Donkey anti-Rabbit IgG (H+L), Alexa Fluor Plus 555	Donkey	1:1,000	A32794	Invitrogen
Donkey anti-Mouse IgG (H+L), Alexa Fluor Plus 647	Donkey	1:1,000	A32787	Invitrogen

Table S4. List of primary antibodies used for western blot analyses.

Antibody Name	Host, Isotype and Subclass	Dilution	Catalog No.	Company Name
c-kit	Rabbit	1:1,000	3074	Cell Signaling Technology
TYR	Mouse IgG2a	1:1,000	SC20035	Santa Cruz Biotechnology
Melan-A	Rabbit	1:100	ab51061	Abcam
TRP1	Mouse IgG2a	1:100	sc58438	Santa Cruz Biotechnology
PMEL	Mouse IgG1	1:100	sc377325	Santa Cruz Biotechnology
DCT	Mouse IgG2a	1:100	sc74439	Santa Cruz Biotechnology
RhoA	Rabbit	1:1,000	2117	Cell Signaling Technology
RAC1/2/3	Rabbit	1:1,000	2465	Cell Signaling Technology
CDC42	Rabbit	1:1,000	2462	Cell Signaling Technology
F-actin	Mouse IgM	1:100	ab205	Abcam
YAP	Rabbit	1:1,000	8418	Cell Signaling Technology
CCN1	Rabbit	1:1,000	14479	Cell Signaling Technology
CCN2	Rabbit	1:1,000	86641	Cell Signaling Technology
BRAF	Rabbit	1:1,000	9433	Cell Signaling Technology
Erk	Rabbit	1:1,000	4695	Cell Signaling Technology
p-Erk	Rabbit	1:1,000	4370	Cell Signaling Technology
p38	Rabbit	1:1,000	8690	Cell Signaling Technology
p-p38	Rabbit	1:1,000	4511	Cell Signaling Technology
JNK	Rabbit	1:1,000	9252	Cell Signaling Technology
p-JNK	Rabbit	1:1,000	4668	Cell Signaling Technology
c-Jun	Rabbit	1:1,000	9165	Cell Signaling Technology
p-c-Jun	Rabbit	1:1,000	3270	Cell Signaling Technology
c-Fos	Rabbit	1:1,000	4384	Cell Signaling Technology
p-c-Fos	Rabbit	1:1,000	5348	Cell Signaling Technology
JunB	Rabbit	1:1,000	3753	Cell Signaling Technology
p-JunB	Rabbit	1:1,000	8053	Cell Signaling Technology
JunD	Rabbit	1:1,000	5000	Cell Signaling Technology
GAPDH	Rabbit	1:1,000	52118	Cell Signaling Technology

Table S5. List of siRNAs used for siRNA-mediated knockdown in melanocytes.

SiRNA Name	Species	Assay ID	Catalog No.	Company Name
Dystroglycan Silencer® Select	Human	s3908	4394420	Thermo Fisher Scientific
LARGE Silencer® Select	Human	s17620	4392420	Thermo Fisher Scientific
Integrin α1 Silencer® Select	Human	s7532	4390824	Thermo Fisher Scientific
Integrin α3 Silencer® Select	Human	s7543	4390824	Thermo Fisher Scientific
Integrin α4 Silencer® Select	Human	s7545	4390824	Thermo Fisher Scientific
Integrin α6 Silencer® Select	Human	s7493	4390824	Thermo Fisher Scientific
Integrin αv Silencer® Select	Human	s7570	4390824	Thermo Fisher Scientific
Integrin β1 Silencer® Select	Human	s7576	4390824	Thermo Fisher Scientific
Integrin β3 Silencer® Select	Human	s7581	4392420	Thermo Fisher Scientific
YAP1 Silencer® Select	Human	s20366	4392420	Thermo Fisher Scientific
TEAD1 Silencer®	Human	116315	AM16708	Thermo Fisher Scientific
CCN1 Silencer® Select	Human	s7244	4390824	Thermo Fisher Scientific
CCN2 Silencer® Select	Human	s3708	4390824	Thermo Fisher Scientific
BRAF Silencer® Select	Human	s2081	4392420	Thermo Fisher Scientific
ERK1 Silencer® Select	Human	s11137	4390824	Thermo Fisher Scientific
JNK1 Silencer® Select	Human	s11152	4392420	Thermo Fisher Scientific
JUN Silencer® Select	Human	s7659	4392420	Thermo Fisher Scientific
CFOS Silencer® Select	Human	s5340	4392420	Thermo Fisher Scientific
PIK3CA Silencer® Select	Human	s10522	4392420	Thermo Fisher Scientific
GSK3B Silencer® Select	Human	s6239	4390824	Thermo Fisher Scientific
CTNNB1 Silencer® Select	Human	s436	4390824	Thermo Fisher Scientific
NOTCH1 Silencer® Select	Human	s453558	4392420	Thermo Fisher Scientific
SOX9 Silencer® Select	Human	s13306	4392420	Thermo Fisher Scientific
MT1-MMP Silencer®	Human	104074	AM51331	Thermo Fisher Scientific
MT4-MMP Silencer®	Human	23831	AM16708	Thermo Fisher Scientific

Table S6. List of compounds used for in vitro drug treatments.

Compound Category	Compound Name	Treatment Concentration	Catalog No.	Company Name
Actin inhibitors	Cytochalasin D	1 μM	034-25881	FUJIFILM Wako Pure Chemical Corporation
	Latrunculin B	250 nM	AG-CN2-0031-M001	AdipoGen Life Sciences
	Chaetoglobosin A	500 nM	BVT-0092-M001	AdipoGen Life Sciences
Actin activator	Jasplakinolide	5 nM	AG-CN2-0037-C100	AdipoGen Life Sciences
Rho/Rac/Cdc42 activator	Rho/Rac/Cdc42 Activator I	2 μg/ml	CN04A	Cytoskeleton, Inc.
ROCK activator	Narciclasine	40 nM	SML2805	Sigma-Aldrich
YAP inhibitors	TED-347	150 nM	HY-125269	MedchemExpress
	Verteporfin	300 nM	HY-B0146	MedchemExpress
YAP activators	PY-60	10 μM	HY-141644	MedchemExpress
	GA-017	10 μM	HY-147082	MedchemExpress
JNK inhibitors	SP600125	50 μM	HY-12041	MedchemExpress
	T-5224	25 μM	HY-12270	MedchemExpress
JNK activator	Anisomycin	100 nM	HY-18982	MedchemExpress

Table S7. List of compounds used for in vivo drug treatments.

Compound Category	Compound Name	Treatment Concentration	Catalog No.	Company Name
Actin inhibitor	Chaetoglobosin A	500 μM	BVT-0092-M001	AdipoGen Life Sciences
Actin activator	Jasplakinolide	10 μM	AG-CN2-0037-C100	AdipoGen Life Sciences
YAP inhibitor	Verteporfin	500 μM	HY-B0146	MedchemExpress
YAP activator	PY-60	500 μM	HY-141644	MedchemExpress
JNK inhibitors	SP600125	500 μM	HY-12041	MedchemExpress
JNK activator	Anisomycin	200 μM	HY-18982	MedchemExpress

Table S8. List of compounds used for ex vivo drug treatments.

Compound Category	Compound Name	Treatment Concentration	Catalog No.	Company Name
Actin inhibitor	Latrunculin B	2 μM	AG-CN2-0031-M001	AdipoGen Life Sciences
	Chaetoglobosin A	7.5 μM	BVT-0092-M001	AdipoGen Life Sciences
Actin activator	Jasplakinolide	50 nM	AG-CN2-0037-C100	AdipoGen Life Sciences
YAP inhibitor	TED-347	1 μM	HY-125269	MedchemExpress
	Verteporfin	1 μM	HY-B0146	MedchemExpress
YAP activator	PY-60	10 μM	HY-141644	MedchemExpress
	GA-017	10 μM	HY-147082	MedchemExpress
JNK inhibitors	SP600125	50 μM	HY-12041	MedchemExpress
	T-5224	25 μM	HY-12270	MedchemExpress
JNK activator	Anisomycin	500 nM	HY-18982	MedchemExpress